https://doi.org/10.1038/s41586-019-1105-7

Developmental origin, functional maintenance and genetic rescue of osteoclasts

Christian E. Jacome-Galarza[1,7], Gulce I. Percin[2,3,7], James T. Muller[1,7], Elvira Mass[1,6,7], Tomi Lazarov[1], Jiri Eitler[2], Martina Rauner[4], Vijay K. Yadav[5], Lucile Crozet[1], Mathieu Bohm[1], Pierre-Louis Loyher[1], Gerard Karsenty[5], Claudia Waskow[2,3,4,8]* & Frederic Geissmann[1,8]*

Osteoclasts are multinucleated giant cells that resorb bone, ensuring development and continuous remodelling of the skeleton and the bone marrow haematopoietic niche. Defective osteoclast activity leads to osteopetrosis and bone marrow failure[1–9], whereas excess activity can contribute to bone loss and osteoporosis[10]. Osteopetrosis can be partially treated by bone marrow transplantation in humans and mice[11–18], consistent with a haematopoietic origin of osteoclasts[13,16,19] and studies that suggest that they develop by fusion of monocytic precursors derived from haematopoietic stem cells in the presence of CSF1 and RANK ligand[1,20]. However, the developmental origin and lifespan of osteoclasts, and the mechanisms that ensure maintenance of osteoclast function throughout life in vivo remain largely unexplored. Here we report that osteoclasts that colonize fetal ossification centres originate from embryonic erythro-myeloid progenitors[21,22]. These erythro-myeloid progenitor-derived osteoclasts are required for normal bone development and tooth eruption. Yet, timely transfusion of haematopoietic-stem-cell-derived monocytic cells in newborn mice is sufficient to rescue bone development in early-onset autosomal recessive osteopetrosis. We also found that the postnatal maintenance of osteoclasts, bone mass and the bone marrow cavity involve iterative fusion of circulating blood monocytic cells with long-lived osteoclast syncytia. As a consequence, parabiosis or transfusion of monocytic cells results in long-term gene transfer in osteoclasts in the absence of haematopoietic-stem-cell chimerism, and can rescue an adult-onset osteopetrotic phenotype caused by cathepsin K deficiency[23,24]. In sum, our results identify the developmental origin of osteoclasts and a mechanism that controls their maintenance in bones after birth. These data suggest strategies to rescue osteoclast deficiency in osteopetrosis and to modulate osteoclast activity in vivo.

In vitro, osteoclasts arise by fusion of haematopoietic stem cell (HSC)-derived precursors and require expression of *Csf1r* and *Tnfrsf11a* (also known as *Rank*). To probe the origin of osteoclasts in vivo we first generated *Csf1r*^{cre};*Csf1r*$^{fl/fl}$ and *Csf1r*^{cre};*Tnfrsf11a*$^{fl/fl}$ mice. These mice presented with an osteopetrotic phenotype similar to *Csf1*$^{op/op}$ (ref. [5]), *Csf1r*[6] and *Tnfrsf11a*[3] mutants, characterized in young mice by a lack of teeth eruption, skull and skeletal deformities with shortness of long bones, increased bone density and lack of osteoclasts and haematopoietic cells (Fig. 1a, Extended Data Fig. 1). To confirm that osteoclast differentiation requires expression of *Tnfrsf11a* and *Csf1r* in HSC-derived precursors, we generated *Flt3*^{cre};*Tnfrsf11a*$^{fl/fl}$, *Flt3*^{cre};*Csf1r*$^{fl/fl}$ and *Vav1*^{cre};*Csf1r*$^{fl/fl}$ mice. The young mutant mice had normal teeth, bone morphology, bone marrow cellularity and osteoclast numbers in comparison to control littermates (Fig. 1b–d, Extended Data Fig. 2). However, *Flt3*^{cre};*Tnfrsf11a*$^{fl/fl}$, *Flt3*^{cre};*Csf1r*$^{fl/fl}$ and *Vav*^{cre};*Csf1r*$^{fl/fl}$ mice lost their osteoclasts over time (Fig. 1d), and by 22–60 weeks of age had increased trabecular bone density (Fig. 1e) and decreased haematopoietic cell numbers in the long bones (Fig. 1c, Extended Data Fig. 2), and 3D X-ray imaging by micro-computed tomography (micro-CT) confirmed the increased bone mass, whereas bone formation—measured by calcein incorporation—was similar to that in control mice (Fig. 1f, Extended Data Fig. 3). In addition, tartrate resistant acid phosphatase-positive (TRAP$^+$) multinucleated cells that appear at embryonic day (E)15 in ossification centres[25] in *Csf1r*^{cre};*Rosa26*$^{LSL\text{-}YFP}$ mice were labelled with YFP, and osteoclasts remained YFP-positive throughout life (Fig. 1g, Extended Data Fig. 4), but gained expression of YFP after birth in *Flt3*^{cre};*Rosa26*$^{LSL\text{-}YFP}$ mice despite colonization of the fetal bone marrow by *Flt3*$^{cre+}$YFP$^+$ haematopoietic cells (Fig. 1h, Extended Data Fig. 4).

These data suggested that although postnatal contribution of HSC-derived cells is important for optimal osteoclast maintenance and function in adults and ageing mice, osteoclast development, tooth eruption and the development of bone and the bone marrow cavity require precursors that are independent from the HSC lineage. These precursors may originate from the embryonic erythro-myeloid progenitor (EMP) lineage of resident macrophages[22,26,27], because *Csf1r*^{cre} mice enable deletion of target genes in both the embryonic EMP lineage and in the HSC lineage, whereas *Flt3*^{cre} (refs [22,26]) and *Vav*^{cre} (Extended Data Fig. 5) are not expressed in the EMP lineage. In support of this hypothesis, we found that TRAP$^+$ multinucleated cells develop in ossification centres from *Myb*-deficient embryos around E15; at this stage the embryos lack HSCs but still support the development of EMP-derived macrophages[26] (Fig. 2a, b). In addition, TRAP$^+$ multinucleated cells are labelled with YFP in tamoxifen-inducible *Csf1r*$^{Mer\text{-}icre\text{-}Mer}$;*Rosa26*$^{LSL\text{-}YFP}$ mice pulsed at E8.5 with a single dose of hydroxytamoxifen (4-OHT), which labels EMPs but not HSCs[22,26,27] (Fig. 2c, d, Extended Data Fig. 4). Together, these results indicate that fetal osteoclasts arise from EMPs in ossification centres.

We therefore investigated whether EMPs are required for bone development. *Tnfrsf11a* is expressed by osteoclasts, but its expression is also a hallmark of EMP-derived macrophage precursors that colonize the developing embryo[27]. In two independent lines of *Tnfrsf11a*^{cre} knock-in mice, referred to as 'Koba' and 'Wask'(Fig. 2e–j), Cre-mediated expression of a *Rosa26*$^{LSL\text{-}YFP}$ fluorescent reporter occurs with high efficiency in fetal macrophages but with low efficiency[27] or not at all[28] in HSCs and their progeny in blood and tissues[27,28] (Extended Data Fig. 5). We therefore hypothesized that conditional deletion of *Csf1r* in *Tnfrsf11a*^{cre} mice would recapitulate the macrophage deficiency observed in *Csf1r*-deficient mice[6], while leaving the HSC lineage unaffected. To test osteoclast and bone development in this model, we generated *Tnfrsf11a*^{cre};*Csf1r*$^{fl/fl}$ mice (Fig. 2e–j). *Tnfrsf11a*^{cre};*Csf1r*$^{fl/fl}$ mice lacked tissue macrophages such as brain microglia and epidermal Langerhans cells at birth, whereas development of HSCs and blood

[1]Immunology Program, Sloan Kettering Institute, Memorial Sloan Kettering Cancer Center, New York, NY, USA. [2]Regeneration in Hematopoiesis and Animal Models in Hematopoiesis, Institute for Immunology, Dresden, Germany. [3]Regeneration in Hematopoiesis, Leibniz Institute on Aging—Fritz Lipmann Institute (FLI), Faculty of Biological Sciences, Friedrich-Schiller University, Jena, Germany. [4]Department of Medicine III, Faculty of Medicine, Dresden, Germany. [5]Department of Genetics and Development, Columbia University Medical Center, New York, NY, USA. [6]Present address: Developmental Biology of the Innate Immune System, LIMES Institute, University of Bonn, Bonn, Germany. [7]These authors contributed equally: Christian E. Jacome-Galarza, Gulce I. Percin, James T. Muller, Elvira Mass. [8]These authors jointly supervised this work: Claudia Waskow, Frederic Geissmann. *e-mail: claudia.waskow@leibniz-fli.de; geissmaf@mskcc.org

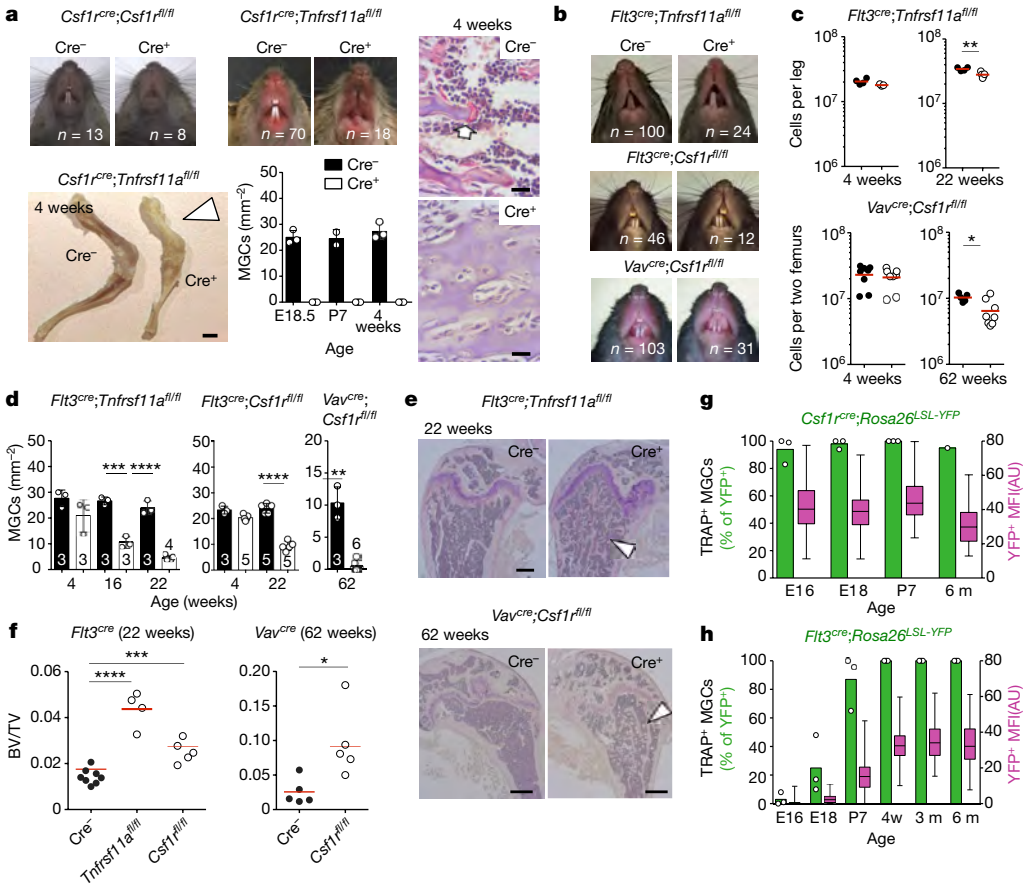

Fig. 1 | HSC-derived precursors are dispensable for osteoclasts and bone development. a, Representative photographs of teeth of three-to-four-week-old *Csf1r*^{cre};*Csf1r*$^{fl/fl}$ mice (top left), *Csf1r*^{cre};*Tnfrsf11a*$^{fl/fl}$ mice (top middle) and control littermates. Bottom left, representative photographs of leg bones from controls and *Csf1r*^{cre};*Tnfrsf11a*$^{fl/fl}$ mice; white arrowhead highlights the lack of blood cells (scale bar, 200 μm). Bottom middle, osteoclast numbers in E18.5, P7 and four-week-old *Csf1r*^{cre};*Tnfrsf11a*$^{fl/fl}$ mice ($n = 3$) and control littermates ($n = 3$), and representative haematoxylin and TRAP staining of femur sections; the arrow indicates an osteoclast (right; scale bar, 20 μm). **b**, Representative photographs of teeth of three-to-four-week-old *Flt3*^{cre};*Tnfrsf11a*$^{fl/fl}$, *Flt3*^{cre};*Csf1r*$^{fl/fl}$, *Vav*^{cre};*Csf1r*$^{fl/fl}$ mice and littermates. **c**, Bone marrow CD45$^+$ cell numbers in *Flt3*^{cre};*Tnfrsf11a*$^{fl/fl}$ and control littermates at 4 (top left, $n = 4$ *Flt3*^{cre};*Tnfrsf11a*$^{fl/fl}$, $n = 3$ control) and 22 weeks of age (top right; $n = 4$ *Flt3*^{cre};*Tnfrsf11a*$^{fl/fl}$, $n = 5$ control) and *Vav*^{cre};*Csf1r*$^{fl/fl}$ and control littermates at 4 (bottom left; $n = 8$ *Vav*^{cre};*Csf1r*$^{fl/fl}$, $n = 8$ control) and 62 weeks of age (bottom right; $n = 5$ *Vav*^{cre};*Csf1r*$^{fl/fl}$, $n = 8$ control). Black, Cre$^-$; white, Cre$^+$. **d**, Osteoclast counts in femurs from *Flt3*^{cre};*Tnfrsf11a*$^{fl/fl}$ (left), *Flt3*^{cre};*Csf1r*$^{fl/fl}$ (middle) and *Vav*^{cre};*Csf1r*$^{fl/fl}$ (right) mice and control littermates of the indicated ages. Number of mice is indicated on individual bars. **e**, Representative haematoxylin and TRAP staining of femur sections from 22-week-old *Flt3*^{cre};*Tnfrsf11a*$^{fl/fl}$ mice (top), 62-week-old *Vav*$^{DD/cre}$;*Csf1r*$^{fl/fl}$ mice (bottom) and control littermates. The white arrowhead points to trabecular bone. Scale bar, 500 μm. **f**, Quantitative analysis of bone volume/total volume of humerus or femurs from *Flt3*^{cre};*Tnfrsf11a*$^{fl/fl}$ ($n = 4$), *Flt3*^{cre};*Csf1r*$^{fl/fl}$ ($n = 5$) and control littermates ($n = 8$), and *Vav*^{cre};*Csf1r*$^{fl/fl}$ ($n = 5$) mice and control littermates ($n = 5$) as determined by micro-CT. *P* values were determined by ANOVA. **g**, Expression and mean fluorescence intensity (MFI) of YFP in TRAP$^+$ multinucleated cells from *Csf1r*^{cre};*Rosa26*$^{LSL\text{-}YFP}$ mice at E16.5, E18.5, P7 and six months ($n = 3$ per time point). For MFI and percentages, at least 100 osteoclasts were quantified per time point and genotype. Box plots show the median, box edges show the first and third quartiles and whiskers show the minimum and maximum. **h**, Similar analysis as in **g**, for *Flt3*^{cre};*Rosa26*$^{LSL\text{-}YFP}$ mice at E16.5, E18.5, P7, 4 weeks (4 w), 3 months (3 m) and 6 months (6 m). Data are mean ± s.d.; dots in graphs represent individual independent biological replicates; *n* indicates the number of mice per group. Statistical significance was analysed with GraphPad Prism using unpaired two-tailed *t*-tests unless otherwise indicated. $^*P < 0.05$, $^{**}P < 0.01$, $^{***}P < 0.001$ and $^{****}P < 0.0001$.

cells was preserved (Extended Data Fig. 2). They exhibited a severe osteopetrotic phenotype, including a lack of tooth eruption (Fig. 2e), misshaped skulls and shorter long bones (Fig. 2 f–h, Extended Data Fig. 1) with few osteoclasts (Fig. 2i) and increased bone density, and initially lacked a bone marrow cavity (Fig. 2f, Extended Data Fig. 2). In contrast to *Csf1r*-deficient mice, however, osteoclasts and haematopoietic cells progressively colonized the long bones of *Tnfrsf11a*^{cre};*Csf1r*$^{fl/fl}$ mice during the first month of life (Fig. 2i, Extended Data Figs. 1, 2), although the mice remained toothless and skull and long-bone deformity persisted (Fig. 2e–h, Extended Data Fig. 1). Calcein incorporation was similar in *Tnfrsf11a*^{cre};*Csf1r*$^{fl/fl}$ mice and their littermate controls (Extended Data Fig. 6). In a complementary approach, ablation of *Csf1r* expression in E10.5 embryos using a single dose of tamoxifen in *Rosa26-creER*$^{T2+}$;*Csf1r*$^{fl/-}$ mice resulted in defective tooth eruption in 3 out of 4 pups at 21 days of age (Extended Data Fig. 5). Together, these analyses support a model in which EMP-derived embryonic osteoclasts are needed for teeth eruption, normal skull shape, optimal formation of long bones and the timely colonization of long bones by haematopoietic progenitors, whereas HSC-derived osteoclasts are important for the maintenance of bone mass after birth and later in life, although they may partially rescue bone development in the absence of EMP-derived osteoclasts in *Tnfrsf11a*^{cre};*Csf1r*$^{fl/fl}$ mice.

To probe the mechanisms that underlie the contribution of HSC-derived blood cells to osteoclast maintenance as well as the lifespan and dynamics of osteoclasts in vivo, we performed time-course parabiosis experiments (Fig. 3a). After four-to-eight weeks of shared blood circulation between *Csf1r*^{cre};*Rosa26*$^{LSL\text{-}YFP}$ and *Csf1r*^{cre};*Rosa26*$^{LSL\text{-}tdTomato}$ parabionts, all osteoclasts—defined as TRAP$^+$ multinucleated cells lining the bone surface—expressed both YFP and tdTomato (Fig. 3a, b). No other cell type was found to co-express YFP and tdTomato in bones

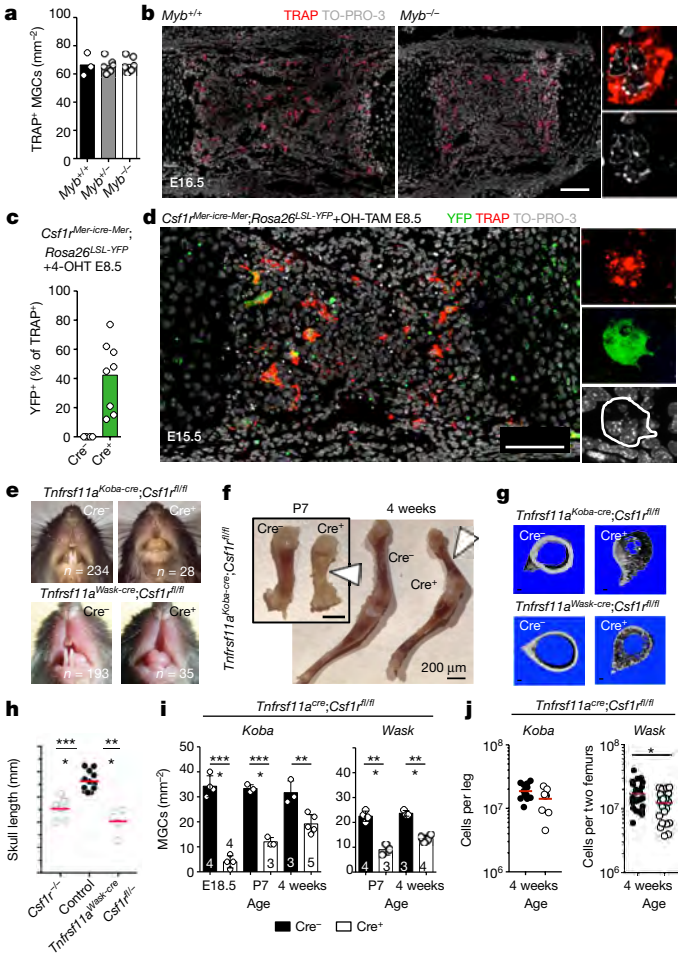

Fig. 2 | EMP-derived osteoclasts are required for bone development. **a**, Multinuclear giant cell (MGC) number in femur anlage ossification centres from E15.5–16.5 $Myb^{-/-}$ ($n = 6$) and littermate controls ($n = 3$). **b**, Representative confocal microscopy of frozen sections from the ossification centres in **a**, stained for TRAP and with TO-PRO-3 nuclear stain. Scale bar, 100 μm. **c**, Percentage of $TRAP^+$ cells expressing YFP in femur anlage from E15.5 $Csf1r^{Mer\text{-}icre\text{-}Mer}$;$Rosa26^{LSL\text{-}YFP}$ mice ($n = 8$) and Cre-negative controls ($n = 5$), pulsed at E8.5 with 4-OHT. **d**, Representative confocal microscopy of a sample from **c**. Scale bar, 100 μm. **e**, Representative teeth of Cre^+ $Tnfrsf11a^{Koba\text{-}cre}$;$Csf1r^{fl/fl}$ (top) and $Tnfrsf11a^{Wask\text{-}cre}$;$Csf1r^{fl/-}$ mice (bottom) and Cre^- control littermates. **f**, Leg bones from $Tnfrsf11a^{cre}$;$Csf1r^{fl/fl}$ mice (Cre^+, $n = 6$) and control littermates (Cre^-, $n = 6$) at P7 and 4 weeks of age. Arrowhead highlights the colour of an area of bone. Scale bar, 200 μm. **g**, Representative micro-CT scans of long bones from mice in **e** ($n = 6$ per genotype). **h**, Skull length from three-week-old $Csf1r^{-/-}$ ($n = 6$) control littermates ($n = 12$) and $Tnfrsf11a^{Wask\text{-}cre}$;$Csf1r^{fl/-}$ mice ($n = 4$), as determined by micro-CT. **i**, Osteoclast counts in bone sections from E18.5, P7 and three-to-four-week old $Tnfrsf11a^{cre}$;$Csf1r^{fl/fl}$ mice and littermate controls. **j**, Number of bone marrow $CD45^+$ cells determined by flow cytometry of cells from four-week-old control (Cre^-) littermates, $Tnfrsf11a^{Koba\text{-}cre}$;$Csf1r^{fl/fl}$ ($n = 9$; $n = 13$ control) and $Tnfrsf11a^{Wask\text{-}cre}$;$Csf1r^{fl/-}$ ($n = 23$, $n = 27$ control) mice (Cre^+). Data are mean ± s.d.; dots in graphs represent individual mice; n indicates the number of mice per group; unpaired two-tailed t-tests. $^*P < 0.05$, $^{**}P < 0.01$, $^{***}P < 0.001$ and $^{****}P < 0.0001$.

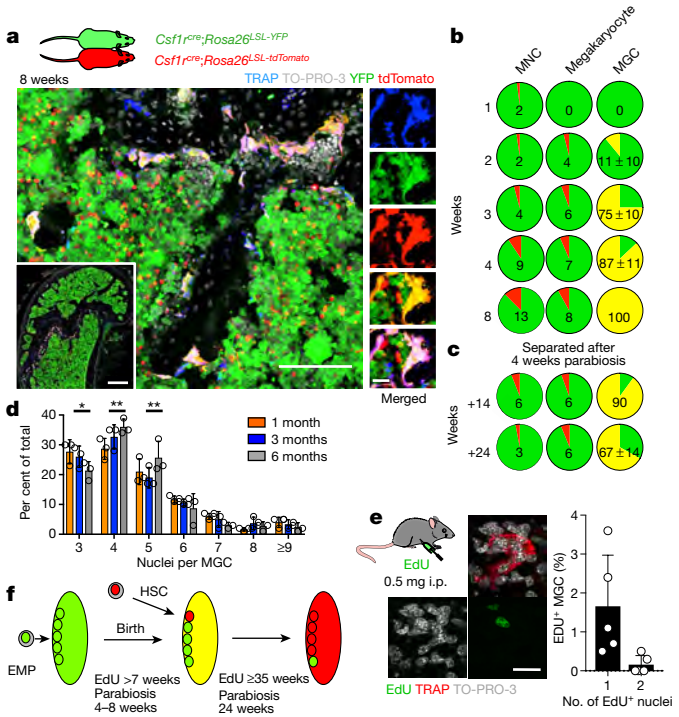

Fig. 3 | In vivo dynamics of osteoclasts. **a**, Parabiosis of $Csf1r^{cre}$;$Rosa26^{LSL\text{-}YFP}$ mouse surgically paired with a $Csf1r^{cre}$;$Rosa26^{LSL\text{-}tdTomato}$ partner for four-to-eight weeks. Representative confocal microscopy of frozen sections from the femur of a $Csf1r^{cre}$;$Rosa26^{LSL\text{-}YFP}$ partner stained with antibodies for tdTomato (red) and YFP (green), ELF 97 (blue) and TOPRO-3 (grey). $n = 3$. Scale bars: 100 μm (left), 500 μm (inset), 20 μm (right). **b**, Pie graphs showing the percentage of $tdTomato^+$ (red), YFP^+ (green) and $tdTomato^+YFP^+$ cells (yellow) among bone marrow mononuclear cells (MNC), megakaryocytes and MGCs from parabionts paired for the indicated time ($n = 8$). **c**, Similar analysis as in **b** for parabionts separated after 4 weeks and analysed 14 and 24 weeks after separation ($n = 3$). **d**, Bar graph showing number of nuclei per $TRAP^+$ MGC in femurs from wild-type mice at one, three and six months of age ($n = 3$ mice per time point). **e**, Representative confocal microscopy of an EdU-labelled nucleus in a $TRAP^+$ osteoclast (left) and histogram showing the percentage of $TRAP^+$ osteoclasts with EdU-labelled nuclei and the number of labelled nuclei per cell 72 h after intravenous pulse-labelling with EdU ($n = 5$ mice). Scale bar, 20 μm **f**, A model for development and maintenance of osteoclast syncytia. Data are mean ± s.d.; dots in graphs represent individual mice; n indicates the number of mice per group; two-way ANOVA with Tukey's multiple comparisons test $^*P \leq 0.05$ and $^{**}P \leq 0.005$.

(Fig. 3b). This is consistent with the presence of nuclei from both partners in individual osteoclasts. Moreover, when parabionts were separated after 4 weeks (Fig. 3c), most recipient YFP^+ osteoclasts retained tdTomato staining 14 weeks after separation, and 2/3 of osteoclasts from former parabionts still expressed both YFP and tdTomato 24 weeks after separation (Fig. 3c). tdTomato signal intensity per YFP osteoclast increased during the eight-week period of shared blood circulation, and decreased after separation (Extended Data Fig. 7). Most mouse osteoclasts contained around five (range from three to seven) nuclei, with a modest increase of nuclei number per cell between one and six months of age (Fig. 3d). These data therefore suggest that individual osteoclast syncytia are long-lived, but acquire new nuclei one at a time every four to eight weeks, from circulating blood cells; it therefore takes more than six months to renew all five nuclei in an individual osteoclast.

We calculated the number and fusion rate of HSC-derived nuclei acquired by osteoclasts in short-term 5-ethynyl-2′-deoxyuridine (EdU)-incorporation studies. A single intravenous pulse of EdU (20 μg g^{-1}) labelled mitotic nuclei and was bioavailable in the bone marrow for around 90 min; approximately 50% of bone marrow and blood monocytic cells were EdU^+ for around 48 h (Extended Data Fig. 7). We observed that approximately 1–2% of osteoclasts were labelled after 72 h, with only 1 EdU^+ nucleus per osteoclast in 90% of EdU^+ cells (Fig. 3e), which suggests that osteoclasts acquire a single postmitotic nucleus at a time. In this model, 0.5–2% of osteoclasts per day acquire a new nucleus, compatible with individual nuclei being

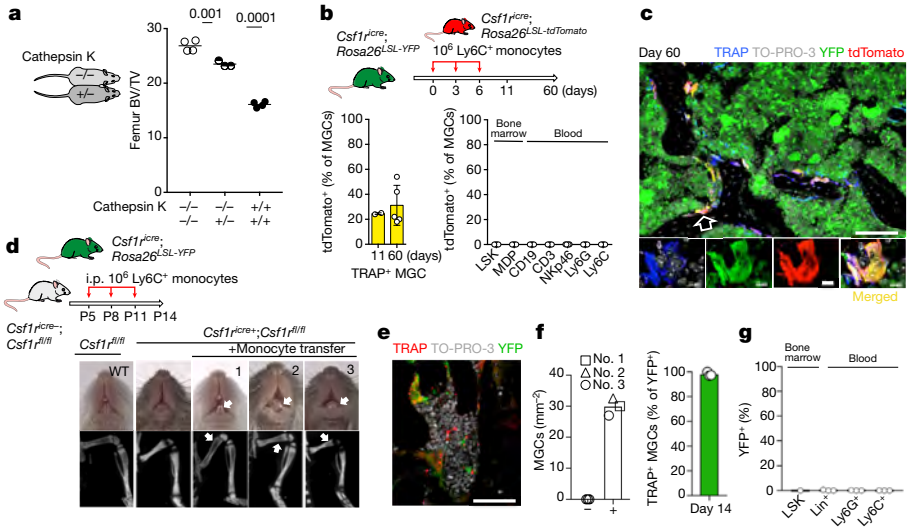

Fig. 4 | Rescue of osteopetrosis. a, Bone volume/total volume for femurs from 10-week-old cathepsin $K^{-/-}$ mice ($n = 3$) after six weeks parabiosis with cathepsin $K^{+/-}$ mice and from positive ($n = 4$) and negative ($n = 4$) control parabionts, analysed by von Kossa staining. **b**, Monocyte transfer. Histograms represent percentage of tdTomato$^+$ cells among bone TRAP$^+$ MGCs from *Csf1r*^{cre};*Rosa26*$^{LSL\text{-}YFP}$ recipients analysed by confocal microscopy (left) 11 days ($n = 2$) and 60 days ($n = 5$) after intravenous transfer at six weeks of age of 3×10^6 Ly6C$^+$ bone marrow cells from *Csf1r*^{cre};*Rosa26*$^{LSL\text{-}tdTomato}$ donors, and percentages of tdTomato$^+$ cells among bone marrow precursors and blood leukocytes, analysed by flow cytometry after 60 days ($n = 5$, right). **c**, Representative high-power confocal microscopy of the femur of a recipient mouse 60 days after intravenous transfer (from **b**), stained with antibodies for tdTomato and YFP, ELF97 phosphatase substrate and TOPRO-3. Scale bars: 100 μm (top), 10 μm (bottom). **d**, Representative photographs of teeth (top) and CT scan of leg bones from *Csf1r*^{cre};*Csf1r*$^{fl/fl}$ mice ($n = 3$) transferred with monocytic cells from *Csf1r*^{cre};*Rosa26*$^{LSL\text{-}YFP}$ donors at P5, P8 and P11, and from wild-type and non-transferred *Csf1r*^{cre};*Csf1r*$^{fl/fl}$ controls. Arrows indicate the presence of teeth eruption (top panels) and bone marrow cavity (bottom panels). **e**, Representative confocal microscopy of a femur from mouse no. 3 in **d**, stained with YFP antibody and with ELF97 and TOPRO-3. Scale bar, 50 μm. **f**, Number of TRAP$^+$ osteoclasts in bone sections from mice in **d** and non-transferred controls (left), and percentage of YFP$^+$TRAP$^+$ cells in transferred mice. The different symbols represent individual mice. Mean values for three sections per mouse. At least 100 osteoclasts were quantified per mouse. **g**, Percentages of YFP$^+$ cells among bone marrow precursors and blood leukocytes in the recipient mice (from **d**) at the time of analysis. Data are mean ± s.d.; dots in graphs represent individual mice; *n* indicates the number of mice per group; ANOVA with Tukey's multiple comparisons test. $***P < 0.001$ and $****P < 0.0001$.

replaced about every 2 months. Together, these studies suggest a model (Fig. 3f) in which osteoclasts that control skeletal development mature in ossification centres from EMPs, whereas their postnatal maintenance is mediated by the serial acquisition by long-lived syncytia of new nuclei from HSC-derived blood leukocytes, rather than by de novo renewal by lateral fusion or proliferation of osteoclast precursors.

A prediction from this model—consistent with an early observation[29]—is that osteopetrosis due to a recessive mutation that affects osteoclast function may be rescued or prevented through parabiosis with a wild-type partner. Parabiosis experiments between four-week-old cathepsin K-deficient mice, which develop an adult-onset form of osteopetrosis known as pycnodysostosis[23,24], and cathepsin $K^{+/-}$ or cathepsin $K^{-/-}$ littermates, and between wild-type mice as control, showed a reduction of bone volume in ten-week-old cathepsin $K^{-/-}$ mice paired with cathepsin $K^{+/-}$ littermates (Fig. 4a), which suggests that circulating blood cells that carry a wild-type cathepsin K allele are sufficient to reduce bone density. To confirm that expression of a donor-derived gene by recipient osteoclasts results from fusion with monocytic cells circulating in the blood, we performed intravenous injections of KIT$^-$Ly6C$^+$ cells from the bone marrow of *Csf1r*^{cre};*Rosa26*$^{LSL\text{-}tdTomato}$ mice into *Csf1r*^{cre};*Rosa26*$^{LSL\text{-}YFP}$ recipients (Fig. 4b, Extended Data Fig. 8). This resulted in stable expression of tdTomato in 20–40% of osteoclasts 1 week and 8 weeks after transfusion, in the absence of other donor-derived blood cells or bone marrow progenitors (Fig. 4b, c, Extended Data Fig. 8). These results suggest that parabiosis or an appropriate transfusion protocol can achieve expression of a donor-derived gene by recipient osteoclasts in the absence of HSC chimerism, and that this effect can last several months.

Partial rescue of osteopetrosis occurs postnatally in *Tnfrsf11a*^{cre};*Csf1r*$^{fl/fl}$ mice, which suggests that transfusion of monocytic cells may also be able to rescue bone development in early-onset congenital osteopetrosis in the absence of a bone marrow transplantation. Intra-peritoneal injections of KIT$^-$Ly6C$^+$ monocytic cells from *Csf1r*^{cre};*Rosa26*$^{LSL\text{-}YFP}$ mice into *Csf1r*^{cre};*Csf1r*$^{F/F}$ neonates, starting from postnatal day (P)5, resulted in complete or partial rescue of teeth eruption (Fig. 4d) and long-bone development as assessed by computerized tomography (CT) scan, with the development of a bone marrow cavity (Fig. 4d) at day 14 in infant mice from three different litters (Fig. 4d, Extended Data Fig. 9). In these mice, femur histology indicated the presence of numerous YFP$^+$TRAP$^+$ osteoclasts lining the bone (Fig. 4e, f). Histology and flow cytometry analyses showed the lack of YFP$^+$ circulating blood cells or bone marrow progenitors (Fig. 4e, g), indicating the absence of HSC engraftment. These data suggest that transfusion of monocytic cells can rescue bone development in early-onset autosomal recessive osteopetrosis in infant mice, in the absence of HSC transplantation.

In sum, we have shown here that osteoclasts originating from EMPs are essential for normal bone development. Moreover, we show that osteoclasts are long-lived in adults and that their function is maintained by iterative fusion of individual HSC-derived circulating cells with existing syncytia. With absence or deficiency of EMP-derived osteoclasts, however, their timely replacement by transfusion with monocytic cells can rescue bone development in early-onset osteopetrotic mice without bone marrow transplantation. This is of potential clinical relevance because bone marrow and HSC transplantation, the standard treatment for early-onset osteopetrosis in mice and humans[11–18], requires irradiation or chemotherapy—which increases the risk of infections, is frequently performed in patients who already suffer severe complications and has a six-year overall survival rate of approximately 48%[17]. In addition, the original mechanism that mediates osteoclast

maintenance in adult mice suggests that these cells represent a unique target for gene transfer by cellular therapies based on transfusion of wild-type or engineered monocytic cells to modulate osteoclast activity and bone remodelling in adults.

Online content

Any methods, additional references, Nature Research reporting summaries, source data, statements of data availability and associated accession codes are available at https://doi.org/10.1038/s41586-019-1105-7.

Received: 10 April 2018; Accepted: 6 March 2019;
Published online 10 April 2019.

1. Lacey, D. L. et al. Osteoprotegerin ligand is a cytokine that regulates osteoclast differentiation and activation. *Cell* **93**, 165–176 (1998).
2. Kong, Y. Y. et al. OPGL is a key regulator of osteoclastogenesis, lymphocyte development and lymph-node organogenesis. *Nature* **397**, 315–323 (1999).
3. Dougall, W. C. et al. RANK is essential for osteoclast and lymph node development. *Genes Dev.* **13**, 2412–2424 (1999).
4. Hsu, H. et al. Tumor necrosis factor receptor family member RANK mediates osteoclast differentiation and activation induced by osteoprotegerin ligand. *Proc. Natl Acad. Sci. USA* **96**, 3540–3545 (1999).
5. Yoshida, H. et al. The murine mutation osteopetrosis is in the coding region of the macrophage colony stimulating factor gene. *Nature* **345**, 442–444 (1990).
6. Dai, X.-M. et al. Targeted disruption of the mouse colony-stimulating factor 1 receptor gene results in osteopetrosis, mononuclear phagocyte deficiency, increased primitive progenitor cell frequencies, and reproductive defects. *Blood* **99**, 111–120 (2002).
7. Lomaga, M. A. et al. TRAF6 deficiency results in osteopetrosis and defective interleukin-1, CD40, and LPS signaling. *Genes Dev.* **13**, 1015–1024 (1999).
8. Tondravi, M. M. et al. Osteopetrosis in mice lacking haematopoietic transcription factor PU.1. *Nature* **386**, 81–84 (1997).
9. Takayanagi, H. et al. Induction and activation of the transcription factor NFATc1 (NFAT2) integrate RANKL signaling in terminal differentiation of osteoclasts. *Dev. Cell* **3**, 889–901 (2002).
10. Lau, R. Y. & Guo, X. A review on current osteoporosis research: with special focus on disuse bone loss. *J. Osteoporos.* **2011**, 293808 (2011).
11. Coccia, P. F. et al. Successful bone-marrow transplantation for infantile malignant osteopetrosis. *N. Engl. J. Med.* **302**, 701–708 (1980).
12. Sorell, M. et al. Marrow transplantation for juvenile osteopetrosis. *Am. J. Med.* **70**, 1280–1287 (1981).
13. Walker, D. G. Bone resorption restored in osteopetrotic mice by transplants of normal bone marrow and spleen cells. *Science* **190**, 784–785 (1975).
14. Ballet, J. J., Griscelli, C., Coutris, C., Milhaud, G. & Maroteaux, P. Bone-marrow transplantation in osteopetrosis. *Lancet* **2**, 1137 (1977).
15. Nisbet, N. W., Menage, J. & Loutit, J. F. Bone-marrow transplantation in osteopetrosis. *Lancet* **2**, 1236 (1977).
16. Ash, P., Loutit, J. F. & Townsend, K. M. Osteoclasts derived from haematopoietic stem cells. *Nature* **283**, 669–670 (1980).
17. Orchard, P. J. et al. Hematopoietic stem cell transplantation for infantile osteopetrosis. *Blood* **126**, 270–276 (2015).
18. Frattini, A. et al. Rescue of ATPa3-deficient murine malignant osteopetrosis by hematopoietic stem cell transplantation *in utero*. *Proc. Natl Acad. Sci. USA* **102**, 14629–14634 (2005).
19. Jotereau, F. V. & Le Douarin, N. M. The development relationship between osteocytes and osteoclasts: a study using the quail-chick nuclear marker in endochondral ossification. *Dev. Biol.* **63**, 253–265 (1978).
20. Shalhoub, V. et al. Characterization of osteoclast precursors in human blood. *Br. J. Haematol.* **111**, 501–512 (2000).
21. McGrath, K. E. et al. Distinct sources of hematopoietic progenitors emerge before HSCs and provide functional blood cells in the mammalian embryo. *Cell Reports* **11**, 1892–1904 (2015).
22. Gomez Perdiguero, E. et al. Tissue-resident macrophages originate from yolk-sac-derived erythro-myeloid progenitors. *Nature* **518**, 547–551 (2015).
23. Maroteaux, P. & Lamy, M. Pyknodysostosis. *Presse Med.* **70**, 999–1002 (1962).
24. Gelb, B. D., Shi, G. P., Chapman, H. A. & Desnick, R. J. Pycnodysostosis, a lysosomal disease caused by cathepsin K deficiency. *Science* **273**, 1236–1238 (1996).
25. Taniguchi, N. et al. Stage-specific secretion of HMGB1 in cartilage regulates endochondral ossification. *Mol. Cell. Biol.* **27**, 5650–5663 (2007).
26. Schulz, C. et al. A lineage of myeloid cells independent of Myb and hematopoietic stem cells. *Science* **336**, 86–90 (2012).
27. Mass, E. et al. Specification of tissue-resident macrophages during organogenesis. *Science* **353**, aaf4238 (2016).
28. Percin, G. I. et al. CSF1R regulates the dendritic cell pool size in adult mice via embryo-derived tissue-resident macrophages. *Nat. Commun.* **9**, 5279 (2018).
29. Walker, D. G. Osteopetrosis cured by temporary parabiosis. *Science* **180**, 875 (1973).

Acknowledgements This work was supported by a NIH/NCI P30CA008748 MSKCC core grant, NIH/NIAID 1R01AI130345 and NIH/NHLBI R01HL138090 to F.G. and by the German Research Foundation (DFG) through FOR2033-A03, TRR127-A5, WA2837/6-1 and WA2837/7-1 to C.W. The authors thank Y. Kobayashi, J. Pollard, T. Graf, R. Stanley, J. Frampton, T. Boehm and J. Penninger for providing mouse strains, and the MSKCC molecular cytology core for preparation of histological samples. The authors are indebted to R. O'Reilly and F. Boulad for helpful suggestions. F.G. is grateful to G. Ruth for support. This study is dedicated to the memory of Lucile Crozet.

Reviewer information *Nature* thanks Roland Baron, Irving L. Weissmann and Mone Zaidi for their contribution to the peer review of this work.

Author contributions F.G. and C.W. designed the study, supervised experiments and analysed data. F.G. wrote the draft of the manuscript. C.E.J.-G. performed histology and immunofluorescence analyses. E.M. and C.E.J.-G. supervised or performed fate-mapping and genetic deletion experiments with *Csf1r*$^{Mer\text{-}icre\text{-}Mer}$, *Flt3*^{cre}, *Csf1r*^{icre} and *Tnfrsf11a*^{cre}, EdU incorporation studies and adoptive transfer studies. G.I.P. performed lineage tracing and genetic deletion experiments with *Tnfrsf11a*^{cre} and *Vav*^{cre} mice and histomorphometry studies. J.T.M. performed and analysed rescue experiments in *Catk*-deficient mice and *Csf1r*^{cre};*Csf1r*$^{f/f}$ mice. P.-L.L. assisted with parabiosis surgeries. V.K.Y. and G.K. analysed *Catk* parabiosis rescue experiments. J.E. performed inducible genetic deletion experiments in *R26-creER*$^{T2+}$;*Csf1r*$^{F/F}$ embryos. T.L., L.C., G.I.P., M.B. and E.M. performed flow cytometry analyses. M.R. scanned bones using micro-CT, and M.R. and G.I.P. analysed micro-CT data. All authors contributed to the manuscript.

Competing interests F.G. is a consultant and principal investigator on a Sponsored Research Agreement with Third Rock Venture (TRV). The other authors declare no competing interests.

Additional information
Extended data is available for this paper at https://doi.org/10.1038/s41586-019-1105-7.
Supplementary information is available for this paper at https://doi.org/10.1038/s41586-019-1105-7.
Reprints and permissions information is available at http://www.nature.com/reprints.
Correspondence and requests for materials should be addressed to C.W. or F.G.
Publisher's note: Springer Nature remains neutral with regard to jurisdictional claims in published maps and institutional affiliations.

METHODS

Mice. *Csf1r*^{icre} (ref. [30]), *Csf1r*$^{Mer\text{-}icre\text{-}Mer}$ (ref. [31]) and *Csf1r*^{flox} (ref. [32]) mice were provided by J. Pollard, *Csf1r*$^{-/-}$ (ref. [6]) mice by R. Stanley, *Flt3*^{cre} (ref. [33]) mice by T. Boehm, Myb$^{+/-}$ (ref. [34]) mice by J, Frampton and *Vav*^{cre} (ref. [35]) by T. Graf. *Tnfrsf11a*^{flox} mice were provided by J. M. Penninger[36], *Tnfrsf11a*$^{Koba\text{-}cre}$ mice were provided by Y. Kobayashi[37], *Ctsk*$^{tm1(cre)Ska}$ mice[38] were provided M. Ostrowsky (MSKCC) and *Tnfrsf11a*$^{Wask\text{-}cre}$ mice were generated in the Waskow laboratory. *Rosa26-creER*^{T2} (*R26-creER*^{T2})[39] were provided by P. Chambon and A. Berns. *Rosa26*$^{LSL\text{-}YFP}$ (ref. [40]; stock number 006148) and *Rosa26*$^{LSL\text{-}tdTomato}$ (ref. [41]; stock number 007908) reporter mice were purchased from The Jackson Laboratory.

Animal procedures. Mice were bred and kept under specific pathogen conditions in separated ventilated cages in the animal facility of MSKCC and the Medical Theoretical Center of the TU Dresden. All experiments with osteopetrotic mice that lack teeth were performed with mice maximal four weeks of age that were kept with the lactating mother or provided with DietGel 76A (Clear H^2O, 72-07-5022) to avoid secondary effects from malnutrition. Experiments were performed in adherence to the Institutional Review Board (IACUC 15-04-006) from MSKCC and Landesdirektion Dresden and were in compliance with relevant ethical regulations. Mice greater than seven days old were killed by cervical dislocation (TU Dresden), CO_2 asphyxiation or anaesthesia (MSKCC). To collect embryos, pregnant females were euthanized and embryos were collected by postmortem caesarean from the uterus and exsanguinated through decapitation in cold PBS (Fisher, 14190).

Genotyping. PCR genotyping was performed according to protocols that have previously been described[6,30–37,39–41] and indicated in Supplementary Table 1. The investigators were not blinded to allocation during experiments and outcome assessment.

Fate mapping with tamoxifen-inducible Cre models. For timing of embryonic development, mice were crossed at night, the following day a positive vaginal plug was considered as 0.5 days postcoitum (dpc), as previously described[22,26]. Embryos were collected as indicated below. For postnatal time point, pregnant females were monitored for the date of delivery, caesarean sections were carried out at term and neonates were fostered using lactating CD-1 females.

Csf1r$^{Mer\text{-}icre\text{-}Mer}$ female mice were crossed with male *Rosa26*$^{LSL\text{-}YFP/LSL\text{-}YFP}$ mice. Cre recombination in *Csf1r*$^{Mer\text{-}icre\text{-}Mer}$;*Rosa26*$^{LSL\text{-}YFP}$ embryos at E8.5 was induced with a single dose of 4-OHT injected intraperitoneally in pregnant mothers at a dose of 75 μg/g of body weight supplemented with 37.5 μg/g of progesterone as previously described[14]. Cre-mediated recombination in *Rosa26-creER*^{T2} was introduced to pregnant mothers by a single tamoxifen gavage (5 mg) at E10.5, supplemented with progesterone (37.5 μg/g body weight resolved in sunflower seed oil (Sigma-Aldrich)), injected intraperitoneally directly after gavage. To analyse newborn or three-week-old mice, caesarean sections were carried out at term and neonates were fostered using lactating CD-1 females.

Parabiosis. For cellular complementation, female *Csf1r*^{icre} mice were crossed to male *Rosa26*$^{LSL\text{-}YFP/YFP}$ or *Rosa26*$^{LSL\text{-}tdTomato/tdTomato}$ mice. *Csf1r*^{icre};*Rosa26*$^{LSL\text{-}YFP}$ and *Csf1r*^{icre};*Rosa26*$^{LSL\text{-}tdTomato}$ females were used for parabiosis. For rescue of cathepsin K activity, four-week-old female *Ctsk*$^{cre/cre}$ and control littermate mice were used for parabiosis. Parabionts were kept on sulfamethoxazole/trimethoprim (Sulfatrim) diet for up to eight weeks. Ex-parabionts were separated after four weeks for cellular complementation and six weeks for rescue of cathepsin K activity.

Surgical procedure, pre-operative procedure. Weight-matched female partner mice for parabiosis were caged together few days before surgery. One day before the surgery the fur from lateral sides of mice was carefully removed with a trimmer followed by depilatory cream (for 3 min) at the site of surgery and excess of fur was removed with a moist gauze pad. The left side partner was shaved on the right side and vice versa. This procedure was performed under isofluorane-inhalation anaesthesia. Mice were fed with food supplemented with Sulfatrim ad libitum one day before surgery.

Surgery. Mice were anaesthetized intraperitoneally with 150 mg/kg of ketamine and 15 mg/kg of xylazine. Sterile eye lubricant (Paralube Vet Ointment, 17033-211-38) was applied to both eyes to prevent corneal drying during surgery. Following confirmation that a suitable anaesthetic plane (no response to stimulation) had been attained, mice were placed in a supine position on a surgical tray with heat support provided by a heating pad. The surgical site was cleaned 3 times with cotton swabs soaked in povidone-iodine (Betadine) and then with 70% ethanol. Before surgery, 0.2 ml anaesthetic agent bupivacaine (Marcaine 0.25–0.5% solution) was applied locally. Surgery was performed by a longitudinal skin incision on the lateral side of mice, approximately 0.5 cm above the elbow to 0.5 cm below the knee joint. Mice were laid side-by-side in close contact and the ligaments of the two knees and elbows were sutured together using monofilament non-absorbable suture. Then, the skin incisions were closed by apposing and clipping skin to skin of the pair with 9-mm wound clips.

Postoperative procedure. Immediately after surgery, mice were injected subcutaneously with 2 mg/kg meloxicam and 0.5mg/kg buprenorphine and for a maximum of 48 h postoperatively. Mice were provided with Sulfatrim and Hydrogel (clear H_2O, 70-01-5022) in medicups. Wound clips were removed 14 days after surgery under isofluorane anaesthesia.

Parabiosis separation procedure. Mice were anaesthetized and prepared for surgery as indicated above. Mice were separated at the site of parabiosis junction. Using scissors, the skin joining both mice was cut longitudinally. The sutures around the elbows and knees were cut and removed. The resulting wound was closed with 9-mm wound clips. Mice were injected subcutaneously with 2 mg/kg meloxicam and 0.5 mg/kg buprenorphine and for a maximum of 48 h postoperatively. Wound clips were removed 14 days after surgery[42].

Analysis. Bones were prepared for histology on frozen sections as detailed below, and stained with antibodies to detect fluorescent proteins: anti-GFP biotin, anti-RFP (Abcam), fluorescent TRAP staining and TO-PRO-3 as a nuclear stain. Histological sections of 15-μm thickness were scanned by confocal microscopy at 1.5-μm *z* stacks. Sections were quantified for the number of TRAP$^+$ multinuclear cells (more than three nuclei per cell) and YFP and tdTomato expression using Imaris in 3D view and individual *z* stacks. Pictures of the region of interest (area = 2 mm^2) were then generated in .tiff format and analysed by ImageJ software using ROI manager to calculate the mean fluorescence intensity of YFP and tdTomato for individual osteoclasts. For rescue of cathepsin K activity, dissected femurs were fixed in 10% neutral buffered formalin for 24 h. Undecalcified bones were embedded in methyl methacrylate resin, and 7-μm sections were prepared on a rotation microtome. For mineralized bone volume/total volume percentage (BV/TV%), sections were de-plastified and stained with von Kossa reagent (1% silver nitrate/sodium formamide/5% sodium thiosulfate) counterstained with Van Gieson solution.

EdU pulse-labelling. Twelve-week-old C57BL/6N mice (Charles River) were injected intraperitoneally with 25 μg/g of 2.5 mg/ml solution of EdU prepared extemporaneously (Fisher C10420, Click-iT EdU Alexa Fluor 488 Flow Cytometry Assay Kit). Blood, bone marrow and bone samples were collected at 60 h and 72 h after injection and bones were prepared for histology of frozen sections as indicated above for adult mice.

Histology of frozen sections. Frozen sections were cut at 15-μm thickness using cryofilm and stained overnight with rat anti-tubulin (Abcam, ab6160, 1:200) and with secondary goat anti-rat Alexa Fluor 555 (ThermoFisher Scientific A21430), as described below. Sections were washed 3 times with PBS and stained for EdU using Click-iT EdU Alexa Fluor 488 Imaging Assay Kit (Thermo Fisher Scientific, C10337). Click-it reaction: 357.5 μl of 1× Click-it reaction buffer, 40 μl of $CuSO_4$ solution (100 mM), 2.5μl of Alexa Fluor 488 azide solution and 100 μl of reaction buffer additive for 500 μl. Sections were incubated for 45 min at room temperature with 100μl of Click-iT EdU reaction buffer then washed with PBS and stained for fluorescent TRAP (ELF 97) and TO-PRO-3 (nuclear stain). Mounting medium was 75% glycerol in PBS.

Microscopy. Images were acquired using an inverted Zeiss LSM880 laser scanning confocal microscope. Histological sections of 15-μm thickness were tile-scanned as 1.0-μm *z* stacks.

Analysis. Sections were analysed using Imaris in 3D view and individual *z* stacks to quantify the percentage of EdU$^+$TRAP$^+$ multinuclear cells and EdU$^+$ nuclei per individual osteoclast.

Adoptive transfers. Bone marrow monocytes were isolated from 12-to-16-week-old donors. In fate-mapping experiments 1×10^6 total cells from *Csf1r*^{icre};*Rosa26*$^{LSL\text{-}tdTomato}$ mice were transferred at day 0, day 3 and day 6 by retro-orbital injections into recipient *Csf1r*^{icre};*Rosa26*$^{LSL\text{-}YFP}$ age and sex-matched mice. Mice were euthanized at day 11 or day 60 after the first transfer. For rescue of osteoclast activity 1×10^6 total bone marrow monocytes from *Csf1r*^{icre};*Rosa26*$^{LSL\text{-}YFP}$ or *Csf1r*^{icre};*Rosa26*$^{LSL\text{-}tdTomato}$ were transferred intra-peritoneally at P5, P8 and P11. Mice were killed at P14, 5 days after the last transfer. Bone marrow and blood was analysed for the percentage of chimerism. To enrich Ly6C$^+$ cells the Monocyte Isolation Kit (BM) for mouse (MACS Miltenyi Biotec, 130-100-629) was used as indicated by the manufacturer. Cell numbers of Ly6C$^+$ cells were calculated by determining the cell number per ml using a Neubauer chamber in combination with staining for Ly6C analysed by flow cytometry. Bone samples were dissected and prepared for frozen sections as described above and stained for anti-GFP, anti-RFP, fluorescent TRAP and TO-PRO-3. The percentages of YFP$^+$ or Tomato$^+$ multinuclear cells was quantified in femurs of recipients.

Preparation and analysis of bone for histology of paraffin-embedded samples. Bone samples were fixed in 4% formaldehyde (Fisher, 28908) in PBS for 1 day (embryo) or 3 days (postnatal mice) at 4 °C then washed 3 times with PBS and decalcified (for mice older than P7) in a 14% EDTA pH7.1 solution at 4 °C for 5 to 15 days, washed 3 times with PBS and dehydrated in 70% ethanol for 1 day and processed for paraffin sections[43]. Longitudinal sections of femurs were cut at 5-μm thickness using a Leica RM2265 paraffin microtome then place in Superfrost microscope slides, allowed to dry for 48 h and heated in a dry incubator at 65 °C for 1 h, dewaxed and stained for TRAP and haematoxylin.

TRAP-staining protocol. To stain for TRAP, slides were placed in coplin jars and incubated in a 1% (v/v) naphtol–ether substrate solution in basic stock solution for 1 h at 37 °C followed by incubation in a solution containing 2% (v/v) sodium nitrate solution and 2% (v/v) basic fuchsin solution in basic stock solution for 20 min at 37 °C. Slides were rinsed in 3 changes of water then stained with haematoxylin solution (Sigma, GHS332) diluted 1:4 in water for 2 min, washed 3 times with water then dehydrated and mounted in Entellan (Millipore, 107960).

Solutions for TRAP staining. Basic stock solution: 0.92% (w/v) anhydrous sodium acetate (Sigma, S8750), 1.14% (w/v) dibasic dihydrate sodium tartrate (Sigma, S4797) and 0.28% (v/v) glacial acetic acid (Sigma, 537020) in distilled water, pH was adjusted between 4.7 and 5.0 with 5 M sodium hydroxide (Fisher, S318-1). Napthol–ether substrate solution: 2% (w/v) napthol AS-BI phosphate (Sigma, 70482) in 2-ethoxyethanol (Sigma, 256374). Sodium nitrate solution: 4% (w/v) sodium nitrate (Sigma, 237213) in water. Basic fuchsin solution: 5% (w/v) basic fuchsin dye (Sigma, 857343) in 2 N HCL (Fisher, A144-500). Individual images from histological sections of 5-μm thickness were acquired using a Zeiss Axio Laboratory A1 light microscope with a N-Achroplan 2.5×/0.07 M27 (420920-9901) or a N-Achroplan 20×/0.45 M27 (420950-9901) objective. Images were taken in ZEN lite software and exported as .tiff files. Panoramic images were created with the photo-merge tool in Adobe Photoshop CS6. Images of mice were acquired with a dissecting microscope Leica M80 equipped with a Leica IC80 HD camera at 1.0× magnification. The region of interest analysed was the methaphyseal trabecular bone 2 mm below the growth plate. The numbers of $TRAP^+$ multinuclear cells (more than three nuclei per cell), associated to bone tissue, were quantified in ImageJ using the cell counter plugin. Numerical values were plotted using GraphPad Prism.

Static and dynamic histomorphometry. Young and aged mice were injected intraperitoneally twice with 15 mg/kg body weight calcein (Sigma) dissolved in 1.4% $NaHCO_3$ in PBS 2 and 3 days apart, respectively. Mice were euthanized two days after the last calcein injection. Femora and tibiae were fixed in 4% PBS-buffered paraformaldehyde and dehydrated in an ascending ethanol series. Subsequently, bones were embedded in methacrylate and cut into 7-μm sections to assess the fluorescent calcein labels. Unstained sections were analysed using fluorescence microscopy to determine the mineralized surface/bone surface, the mineral apposition rate, and the bone formation rate/bone surface. To determine numbers of osteoclasts, bones were decalcified for one week using Osteosoft (Merck), dehydrated and embedded into paraffin. TRAP staining was used to assess the osteoclast surface per bone surface and number of osteoclasts per bone surface. Bone sections were analysed using Osteomeasure software (Osteometrics) following international standards.

Preparation of and analysis of bones for immunofluorescence on frozen sections. Samples were prepared as above and after decalcification and washing were soaked in 30% sucrose in PBS at 4 °C for 1–2 days[43]. Tissue samples were placed in disposable histology plastic moulds and embedded in FSC22 Frozen Section Compound Clear (Leica, 3801480) and placed on a flat surface of dry ice and allowed to freeze.

Immunofluorescence. Bones were cut at 15-μm thickness using a Cryostat Leica CM3050S with high-profile microtome blades (Leica Surgipath DB80 HS) and cryofilm (Section Laboratory) and allowed to dry for 48 h at 4 °C. Before staining with antibodies, sections were allowed to equilibrate at room temperature for 30 min, rehydrated with PBS (Fisher, 14190) 3 times for 5 min at room temperature. Sections were incubated with blocking buffer containing 0.25% BSA (Fisher BP1600), 10% normal goat serum (Life Technologies, PCN 5000) and 0.3% triton (Sigma, T8787) in PBS for 1 h at room temperature. Sections were washed 2 times with PBS for 5 min. Sections stained with anti-GFP biotin antibody were first incubated with biotin–streptavidin blocking kit (Vector laboratories, SP2002). Streptavidin blocking solution is prepared by adding 4 drops of streptavidin solution to 1 ml PBS/0.25% BSA, samples were incubated for 15 min, then washed once with PBS for 5 min. Biotin blocking solution was prepared by adding 4 drops of biotin solution to 1 ml PBS/0.25% BSA; samples were incubated for 15 min then washed once with PBS for 5 min. Primary and secondary antibodies used are listed in Supplementary Table 2. Sections were also stained with fluorescent TRAP and nuclear stain.

TRAP activity. Sections were prepared for fluorescent TRAP staining by incubating with TRAP incubation solution (112 mM sodium acetate, 76 mM sodium tartate and 11 mM sodium nitrite, pH 4.1–4.3) at room temperature for 10 min. Buffer was removed and incubated with ELF97 substrate (Molecular Probes E6589, 2 mM) at a concentration of 125 μM in TRAP incubation solution for 15 min under UV light and washed 2 times with PBS for 5 min[44]. Nuclear stain used was TO-PRO-3 iodide (Fisher T3605) diluted 1:4,000 in PBS for 5 min. Mounting medium was 75% glycerol in PBS. Images were acquired using an inverted Zeiss LSM880 laser scanning confocal microscope with argon-ion 488 nm, diode 405-30 nm, DPSS 561-10 nm, HeNe 633 nm laser lines and Plan-Apochromat 40×/1.4 N.A. DIC (UV) VIS-IR oil objective. Histological sections of 15-μm thickness were tile-scanned at 1.5-μm *z* stacks in ZEN black and processed using ZEN lite. Sections were analysed using Imaris in 3D view and individual *z* stacks to quantify $TRAP^+$ multinuclear cells and YFP and tdTomato labelling. Images of the region of interest were generated in .tiff format and analysed by ImageJ software using ROI manager to calculate the MFI of individual osteoclasts. Numerical values were plotted using GraphPad Prism.

Animal imaging by computed tomography. *NanoSPECT CT.* Mice were anaesthetized under isofluorane anaesthesia and placed on an imaging table containing an animal bed equipped with a nosecone for gas inhalation and body temperature stabilization. For three-week-old mice, a mouse bed was used, and for mice eight weeks and older, a rat bed was used. Whole-body imaging of mice was done using a NanoSPECT CT scanner (Mediso) for non-invasive and longitudinal monitoring of the 3D skeletal structure. Each CT scan averaged 15 min and was acquired with an exposure time of 1,000 ms and 240 projections set at a pitch of 1 degree. The tube energy of the X-ray was 55 KVp and 145 μA. The in-plane voxel size was medium generating a voxel size of 147 μm^3. Reconstructed images were analysed using In vivo Scope 2.0 software (Bioscan).

Micro-CT. For 3D X-ray imaging by micro-CT, mice were euthanized and bones placed in 70% ethanol until scanning. Bone microarchitecture was analysed using a vivaCT40 (Scanco Medical). Entire femora or humeri were imaged at a resolution of 10.5 μm (one slice) with an X-ray energy of 70 kVp, 114 mA, and an integration time of 200 ms. The machine was routinely calibrated using hydroxyapatite phantoms for density and geometry. Trabecular bone in femora or humeri from aged mice was assessed in the metaphysis 20 slices below the growth plate using 150 slices. The trabecular region within the cortical bones (P21 mice) was determined in the femoral midshaft (100 slices up, 100 slices down). Pre-defined scripts from Scanco were used for the evaluation.

Preparation of tissues and staining for flow cytometry. Yolk sacs from E10.5 embryos were digested for 60 min at 37 °C in PBS containing 5% FCS, collagenase type 4 (Worthington, final concentration 4.2 U/ml) and DNaseI (Sigma-Aldrich, final concentration 100 μg/ml). The digestion reaction was stopped by incubation with 12.5 mM EDTA.

Fetal liver was gently dissociated between the frosted ends of glass slides, and was then digested for 30 min using the same digestion enzyme mix as for yolk sac.

Blood was collected from anaesthetized mice by retro-orbital venous sinus bleeding or cardiac puncture using a 1-ml syringe and a 26G needle rinsed with 100 mM EDTA (Sigma E4884). The collected blood was lysed with 3 ml red blood cell lysis buffer (155 mM NH_4Cl (Sigma A9434), 10 mM $NaHCO_3$ (Sigma S5761) and 0.1 mM EDTA (Sigma E4884)) for 5 min, washed with 10 ml FACS buffer (PBS, 0.5% BSA and 2 mM EDTA) and centrifuged at 320*g* for 7 min at 4 °C. All mice were perfused with 10 ml PBS after blood withdrawal.

Bone marrow cells were collected by crushing or flushing femurs and tibias using a syringe and a 26G needle with 10 ml PBS/5% FCS or RPMI supplemented with 10% FBS. Bone marrow was dissociated by gently pipetting up and down with a 1-ml or 10-ml pipette.

Spleens were gently dispersed between frosted slides and digested for 30 min at 37 °C in PBS with 5% FCS containing collagenase type 4 (Worthington) at a final concentration of 4.2 U/ml and 100 μg/ml DNaseI (Sigma-Aldrich). The reaction was stopped by incubation with 12.5 mM EDTA.

Peritoneal cells were collected by flushing the peritoneal cavity with 10 ml PBS/5% FCS heated to 37 °C.

Adult brain and liver were dissected, cut into small fragments and incubated at 37 °C for 30 min in enzyme mix consisting of PBS with 1 mg/ml collagenase D (Sigma, 11088882001), 100 U/ml DNase I (Sigma, DN25), 2.4 mg/ml of dispase (Fisher, 17105-041) and 3% FBS (ThermoFisher Scientific 10438026) or PBS containing 4.2 U/ml collagenase type 4 (Worthington), 100 μg/ml DNaseI, 2.4 mg/ml dispase (Gibco) and 3% FCS at 37 °C for 30 min. After enzyme digestion all tissues were further dissociated by mechanical disruption using 100-μm cell strainers (Falcon, 352360) and a 3-ml syringe plunger in 6-well plates containing 4 ml or 5 ml of cold FACS buffer or PBS/5% FCS. Single-cell suspensions were transferred to 5 ml FACS tubes and pelleted by centrifugation at 320*g* for 7 min at 4 °C. The cell pellets were resuspended in FACS buffer containing purified anti-mouse CD16/32 antibody (1:100, Biolegend 101301), 5% normal mouse (Fisher, 015-000-120), 5% normal rat (Fisher 012-000-120) and 5% normal rabbit (Fisher, 011-000-120) serum, and incubated for 10 min on ice or directly stained using blocking antibodies in the staining mixtures. Samples were immunostained with fluorochrome-conjugated antibodies for 30 min on ice, and analysed by flow cytometry using an LSRFortessa or an LSR II (BD-Bioscience). A full list of antibodies for flow cytometry is provided in Supplementary Table 3. Each sample was stained with Hoechst (ThermoFisher Scientific, Hoechst 33258, 1 μg/ml) or DAPI (Applichem, 1 μg per 25 ml) moments before flow cytometry acquisition.

All analysis was conducted using FlowJo (Tree Star). In all tissues, single live cells were gated by exclusion of dead cells labelled positive by Hoechst or DAPI, side scatter and forward scatter and doublet exclusion using forward-scatter width against forward scatter, as previously described[22,26,27,45,46]. To calculate cell numbers per organ or per gram of tissue, organs were weighed, cell suspensions

were prepared from a weighed amount (20 to 500 mg) of tissue, and the number of cells per gram of tissue was determined using a cell counter (GUAVA easyCyte HT).

Statistical analysis and reproducibility. Data are shown as mean with individual values per mouse represented as dots in graphs, unless stated otherwise. Statistical significance was analysed with GraphPad Prism using unpaired *t*-tests and two-way ANOVA with Tukey's multiple comparisons test as indicated in the figure legends. $*P < 0.05$, $**P < 0.01$, $***P < 0.001$ and $****P < 0.0001$. *n* represents the number of biological replicates. Experiments were repeated to ensure reproducibility of the observations. Equal variance was assumed for cell-counting experiments. No statistical methods were used to predetermine sample size.

Reporting summary. Further information on research design is available in the Nature Research Reporting Summary linked to this paper.

Data availability

Data generated in this study are available from the corresponding author upon reasonable request.

30. Deng, L. et al. A novel mouse model of inflammatory bowel disease links mammalian target of rapamycin-dependent hyperproliferation of colonic epithelium to inflammation-associated tumorigenesis. *Am. J. Pathol.* **176**, 952–967 (2010).
31. Qian, B. Z. et al. CCL2 recruits inflammatory monocytes to facilitate breast-tumour metastasis. *Nature* **475**, 222–225 (2011).
32. Li, J., Chen, K., Zhu, L. & Pollard, J. W. Conditional deletion of the colony stimulating factor-1 receptor (*c-fms* proto-oncogene) in mice. *Genesis* **44**, 328–335 (2006).
33. Benz, C., Martins, V. C., Radtke, F. & Bleul, C. C. The stream of precursors that colonizes the thymus proceeds selectively through the early T lineage precursor stage of T cell development. *J. Exp. Med.* **205**, 1187–1199 (2008).
34. Mucenski, M. L. et al. A functional c-*myb* gene is required for normal murine fetal hepatic hematopoiesis. *Cell* **65**, 677–689 (1991).
35. Stadtfeld, M. & Graf, T. Assessing the role of hematopoietic plasticity for endothelial and hepatocyte development by non-invasive lineage tracing. *Development* **132**, 203–213 (2005).
36. Hanada, R. et al. Central control of fever and female body temperature by RANKL/RANK. *Nature* **462**, 505–509 (2009).
37. Maeda, K. et al. Wnt5a–Ror2 signaling between osteoblast-lineage cells and osteoclast precursors enhances osteoclastogenesis. *Nat. Med.* **18**, 405–412 (2012).
38. Nakamura, T. et al. Estrogen prevents bone loss via estrogen receptor α and induction of Fas ligand in osteoclasts. *Cell* **130**, 811–823 (2007).
39. Hameyer, D. et al. Toxicity of ligand-dependent Cre recombinases and generation of a conditional Cre deleter mouse allowing mosaic recombination in peripheral tissues. *Physiol. Genomics* **31**, 32–41 (2007).
40. Srinivas, S. et al. Cre reporter strains produced by targeted insertion of *EYFP* and *ECFP* into the *ROSA26* locus. *BMC Dev. Biol.* **1**, 4 (2001).
41. Madisen, L. et al. A robust and high-throughput Cre reporting and characterization system for the whole mouse brain. *Nat. Neurosci.* **13**, 133–140 (2010).
42. Kamran, P. et al. Parabiosis in mice: a detailed protocol. *J. Vis. Exp.* **80**, e50556 (2013).
43. Jiang, X. et al. Histological analysis of GFP expression in murine bone. *J. Histochem. Cytochem.* **53**, 593–602 (2005).
44. Filgueira, L. Fluorescence-based staining for tartrate-resistant acidic phosphatase (TRAP) in osteoclasts combined with other fluorescent dyes and protocols. *J. Histochem. Cytochem.* **52**, 411–414 (2004).
45. Arndt, K. et al. SETD1A protects HSCs from activation-induced functional decline in vivo. *Blood* **131**, 1311–1324 (2018).
46. Grinenko, T. et al. Clonal expansion capacity defines two consecutive developmental stages of long-term hematopoietic stem cells. *J. Exp. Med.* **211**, 209–215 (2014).

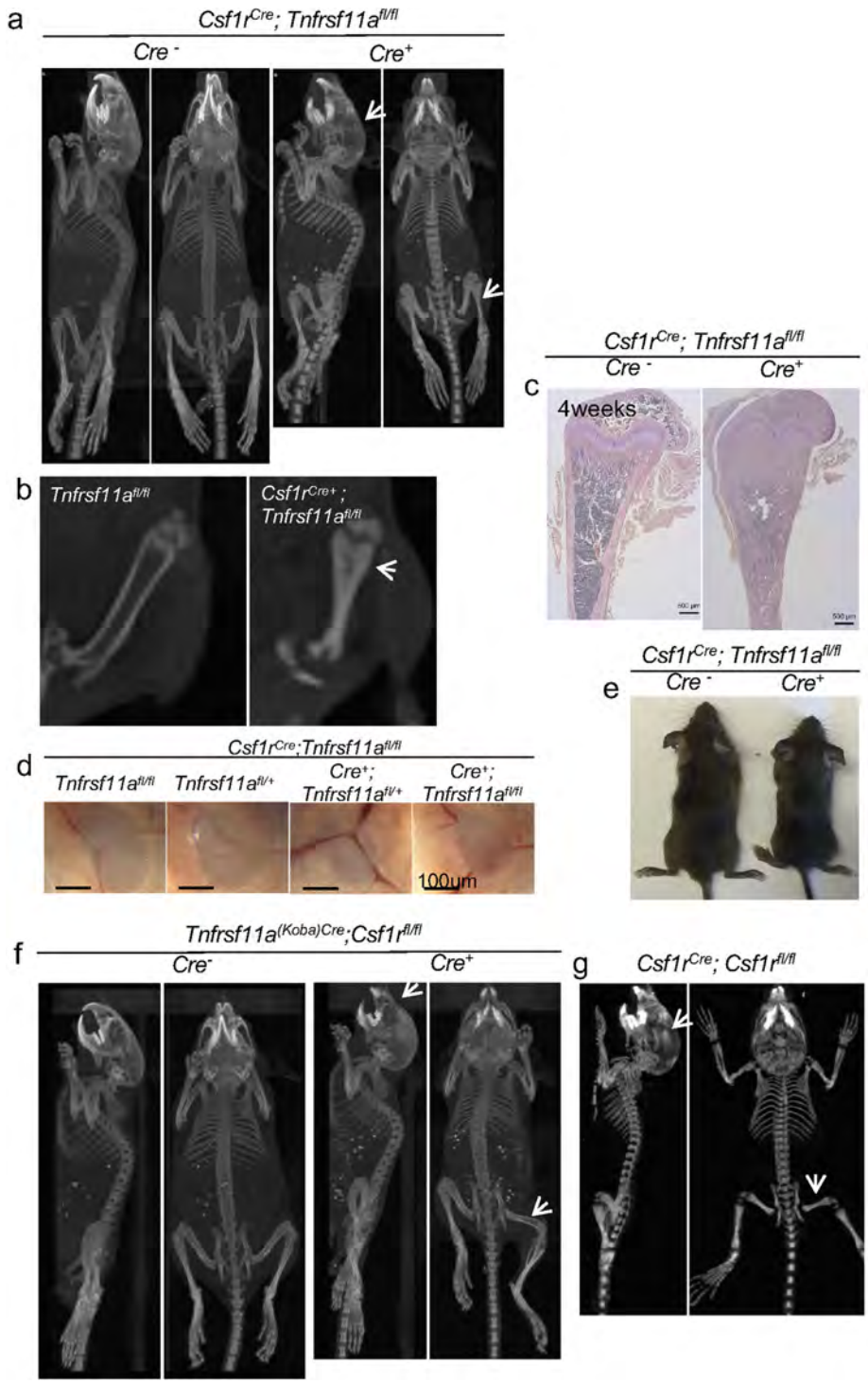

Extended Data Fig. 1 | *Csf1r*^{cre};*Tnfrsf11a*$^{fl/fl}$, *Csf1r*$^{fl/fl}$;*Csf1r*^{cre} and *Tnfrsf11a*^{cre};*Csf1r*$^{fl/fl}$ mice are osteopetrotic. a, **b**, Representative CT scans (nanospect CT) of four-week-old *Csf1r*^{cre};*Tnfrsf11a*$^{fl/fl}$ mice. Arrows indicate skull deformation and absence of bone marrow cavity in mutant mice. **c**, Haematoxylin and TRAP staining of bone sections from four-week-old *Csf1r*^{cre};*Tnfrsf11a*$^{fl/fl}$ mice showing closure of the bone marrow. Histology of paraffin sections (5-μm thickness) corroborates the phenotype from mice in **b**. **d**, Inguinal lymph nodes from *Csf1r*^{cre};*Tnfrsf11a*$^{fl/fl}$ mice. **e**, A representative *Csf1r*^{cre};*Tnfrsf11a*$^{fl/fl}$ and a littermate control. **f**, Representative CT scan reconstructions (nanospect CT) of four-week-old *Tnfrsf11a*$^{Koba\text{-}cre}$;*Csf1r*$^{fl/fl}$ mice. Arrows indicate skull deformation, but with presence of a bone marrow cavity in mutant mice, in contrast to those in **a** and **b**. **g**, Representative CT scans of *Csf1r*^{cre};*Csf1r*$^{fl/fl}$ mice. Arrows indicate skull deformation and absence of bone marrow cavity in mutant mice as in **a** and **b**. CT scans and photographs are representative of >10 litters.

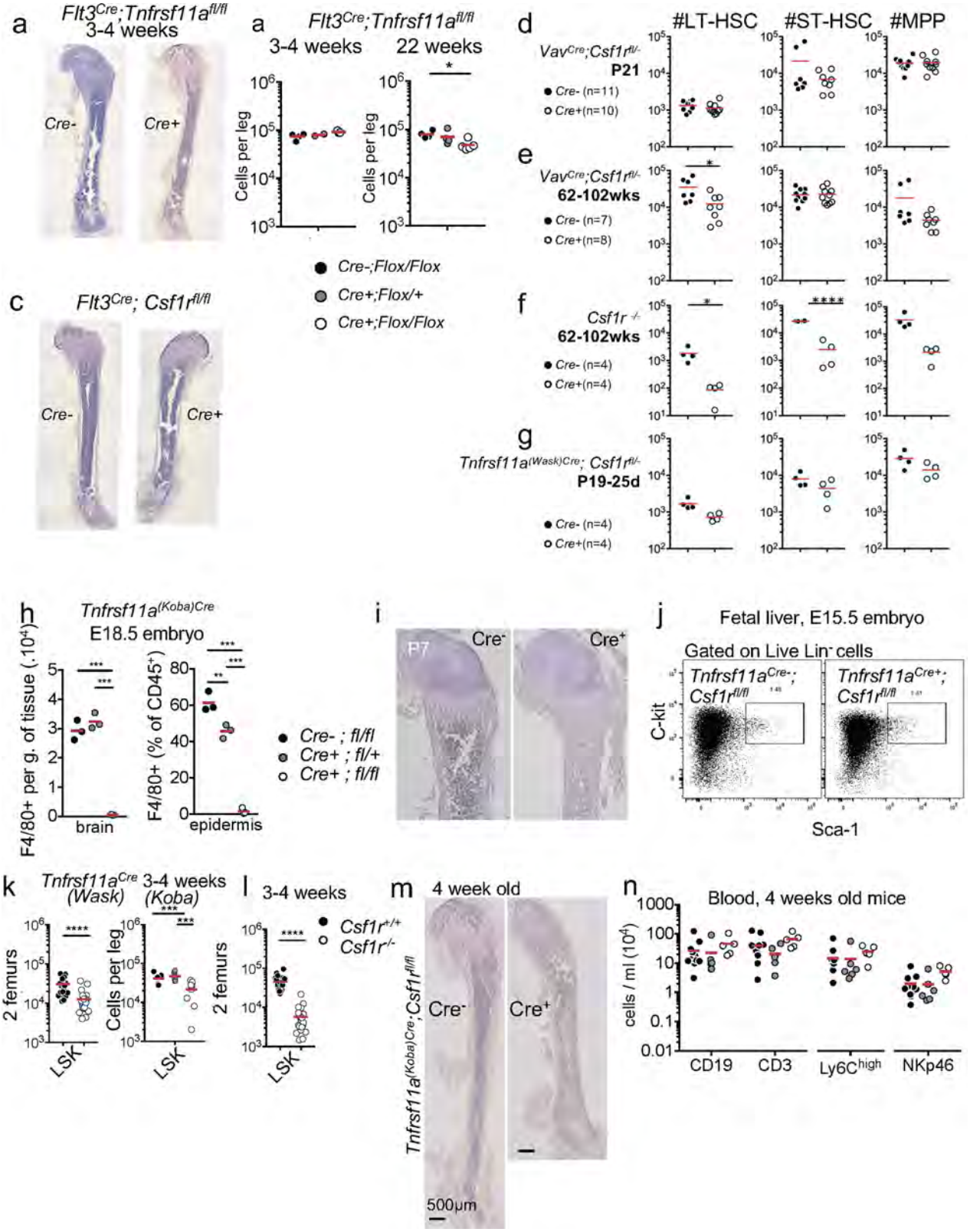

Extended Data Fig. 2 | See next page for caption.

Extended Data Fig. 2 | Bone histology and flow cytometry analysis of bone marrow phenotypic LSK, long-term HSCs, short-term HSCs and multipotent progenitors in mice of indicated genotypes. a, Young *Flt3*^{cre};*Csf1r*$^{fl/fl}$ and *Flt3*^{cre};*Tnfrsf11a*$^{fl/fl}$ mice have normal long bones. Haematoxylin and TRAP staining of bone sections from four-week-old *Flt3*^{cre};*Tnfrsf11a*$^{fl/fl}$ mice, showing normal bone structure and bone marrow cavity. **b**, LSK cell numbers in bone marrow from three-to-four-week-old *Flt3*^{cre};*Tnfrsf11a*$^{fl/fl}$ ($n = 3$) and *Flt3*^{cre};*Tnfrsf11a*$^{fl/+}$ mice ($n = 2$) and littermate controls ($n = 4$) and from 22-week-old *Flt3*^{cre};*Tnfrsf11a*$^{fl/fl}$ ($n = 5$) and *Flt3*^{cre};*Tnfrsf11a*$^{fl/+}$ mice ($n = 4$) and littermate controls ($n = 4$). **c**, Haematoxylin and TRAP staining of bone sections from four-week-old *Flt3*^{cre};*Csf1r*$^{fl/fl}$ mice showing normal bone structure and bone marrow cavity. **d**, **e**, Phenotypic long-term HSCs (LT-HSCs) are reduced in aged wild-type mice but not in young *Vav*^{cre};*Csf1r*$^{fl/-}$ mice. **f**, **g**, LT-HSCs are reduced in in young *Csf1r*$^{-/-}$ mice, and to a lesser extent, in young *Tnfrsf11a*$^{Wask\text{-}cre}$;*Csf1r*$^{fl/-}$ mice. Cell counts for two femurs are shown. **h**, Flow cytometry analysis of F4/80$^+$ cells in brain (microglia) and epidermis (Langerhans cells) in E18.5 *Tnfrsf11a*^{cre};*Csf1r*$^{fl/fl}$ embryos and littermate controls ($n = 3$ per group). **i**, Haematoxylin and TRAP staining of bone sections from P7 *Tnfrsf11a*^{cre};*Csf1r*$^{fl/fl}$ mice and littermate controls, showing absence of the bone marrow cavity. **j**, Flow cytometry of fetal liver at E15.5 (representative results of three experiments). **k**, LSK numbers in bone marrow of three-to-four-week-old *Tnfrsf11a*$^{Wask\text{-}cre}$;*Csf1r*$^{fl/fl}$ mice ($n = 24$) and littermate controls ($n = 20$), and *Tnfrsf11a*$^{Koba\text{-}cre}$;*Csf1r*$^{fl/fl}$ ($n = 7$) and *Tnfrsf11a*$^{Koba\text{-}cre}$;*Csf1r*$^{fl+l}$ mice ($n = 6$) and littermate controls ($n = 8$). **l**, For comparison, LSK numbers in bone marrow of three-to-four-week-old *Csf1r*$^{-/-}$ mice ($n = 22$) and littermate controls ($n = 21$). **m**, Representative micrographs of femur sections from four-week-old *Tnfrsf11a*^{cre};*Csf1r*$^{fl/fl}$ mice and littermate controls, stained with haematoxylin and TRAP. **n**, Blood leukocytes numbers in four-week-old *Tnfrsf11a*^{cre};*Csf1r*$^{fl/fl}$ mice ($n = 5$), *Tnfrsf11a*^{cre};*Csf1r*$^{fl/+}$ mice ($n = 6$) and littermate controls ($n = 12$). Points represent individual mice; results from three independent experiments. Data are mean ± s.d.; *n* indicates the number of mice per group; unpaired two tailed *t*-tests. $^*P < 0.05$, $^{**}P < 0.005$, $^{***}P < 0.0005$ and $^{****}P < 0.0001$. LT-HSC, Lin$^-$KIT$^+$SCA1$^+$;KIT$^+$SCA1$^+$CD34$^-$FLT3$^-$. Phenotypic short-term HSCs (ST-HSC), Lin$^-$KIT$^+$SCA1$^+$CD34$^+$FLT3$^-$. MPP, multipotent progenitors; Lin$^-$KIT$^+$SCA1$^+$CD34$^+$FLT3$^+$. Lin, CD3$^+$CD19$^+$NK1.1$^+$TER119$^+$CD11b$^+$GR1$^+$B220$^+$.

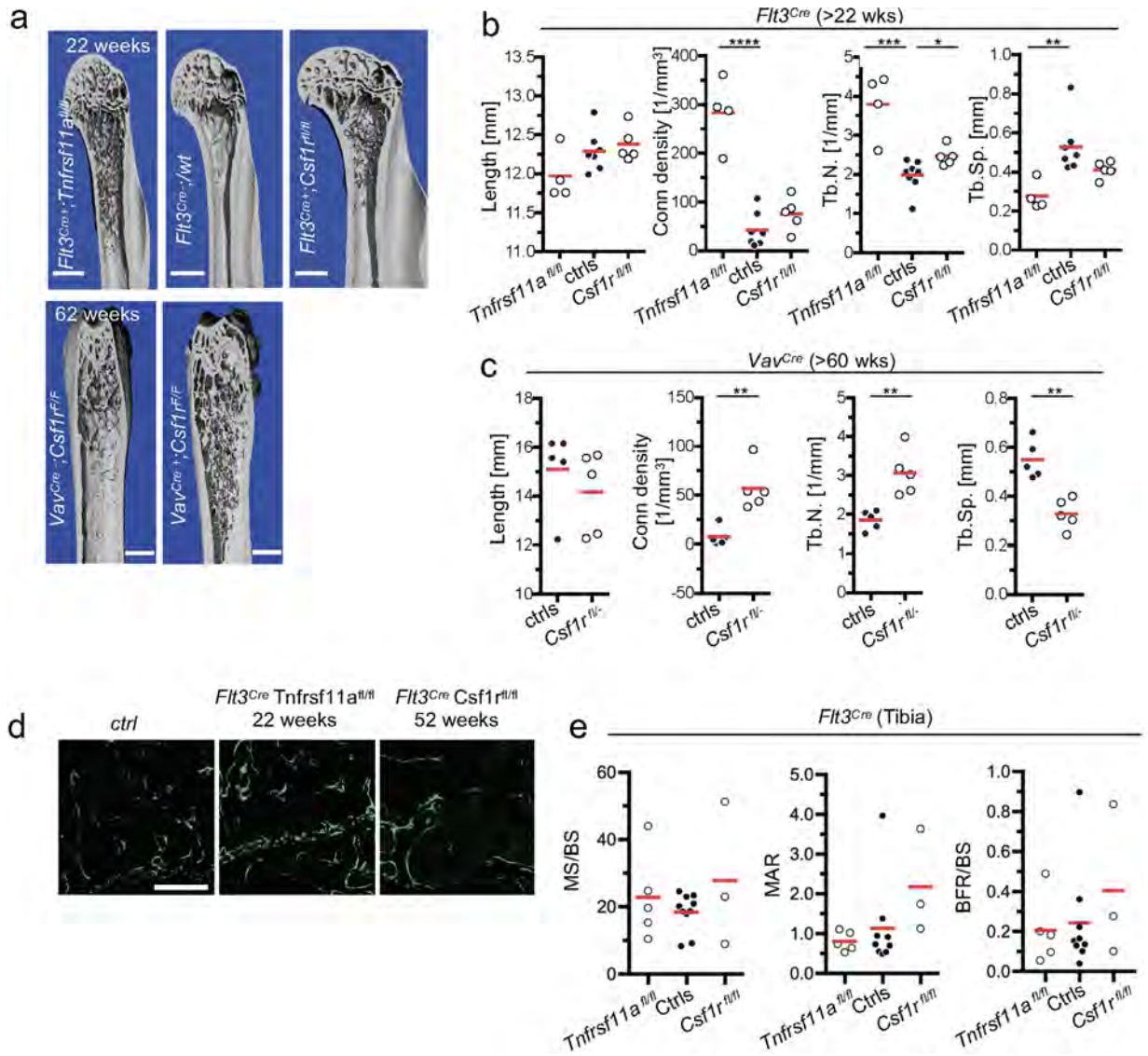

Extended Data Fig. 3 | Bone histomorphometry in aged *Flt3^{cre};Tnfrsf11a$^{fl/fl}$*, *Flt3^{cre};Csf1r$^{fl/fl}$* and *Vav^{cre};Csf1r$^{fl/fl}$* mice and control littermates. a, Representative Micro-CT of humeri (top) and femora (bottom) of mice of the indicated age and genotype. **b**, Bone length, connectivity density (conn density), trabecular number (Tb.N.) and trabecular spacing (Tb.Sp.) analysed by micro-CT in aged *Flt3^{cre};Tnfrsf11a$^{fl/fl}$* ($n = 4$) and *Flt3^{cre};Csf1r$^{fl/fl}$* ($n = 4$) mice and control littermates ($n = 7$). **c**, Bone histomorphometry as in **b**, for *Vav^{cre};Csf1r$^{fl/fl}$* mice and control littermates ($n = 5$). **d**, **e**, Dynamic bone histomorphometry in aged *Flt3^{cre};Tnfrsf11a$^{fl/fl}$* and *Flt3^{cre};Csf1r$^{fl/fl}$* mice using in vivo calcein labelling. **d**, Representative micrographs of calcein labelling (green) of femora of mice from the indicated genotypes and ages. Scale bars: 200 μm (top); 50 μm (bottom). **e**, Quantification of calcein labelling by fluorescence microscopy of mineralized surface/bone surface (MS/BS), mineral apposition rate (MAR) and bone formation rate/bone surface (BFR/BS) in aged *Flt3^{cre};Tnfrsf11a$^{fl/fl}$* ($n = 5$), *Flt3^{cre};Csf1r$^{fl/fl}$* ($n = 3$) and control littermates ($n = 10$) Data are mean ± s.d.; dots in graphs represent individual mice; *n* indicates the number of mice per group; unpaired two tailed *t*-tests. $^{*}P < 0.05$, $^{**}P < 0.005$, $^{***}P < 0.0005$ and $^{****}P < 0.0001$.

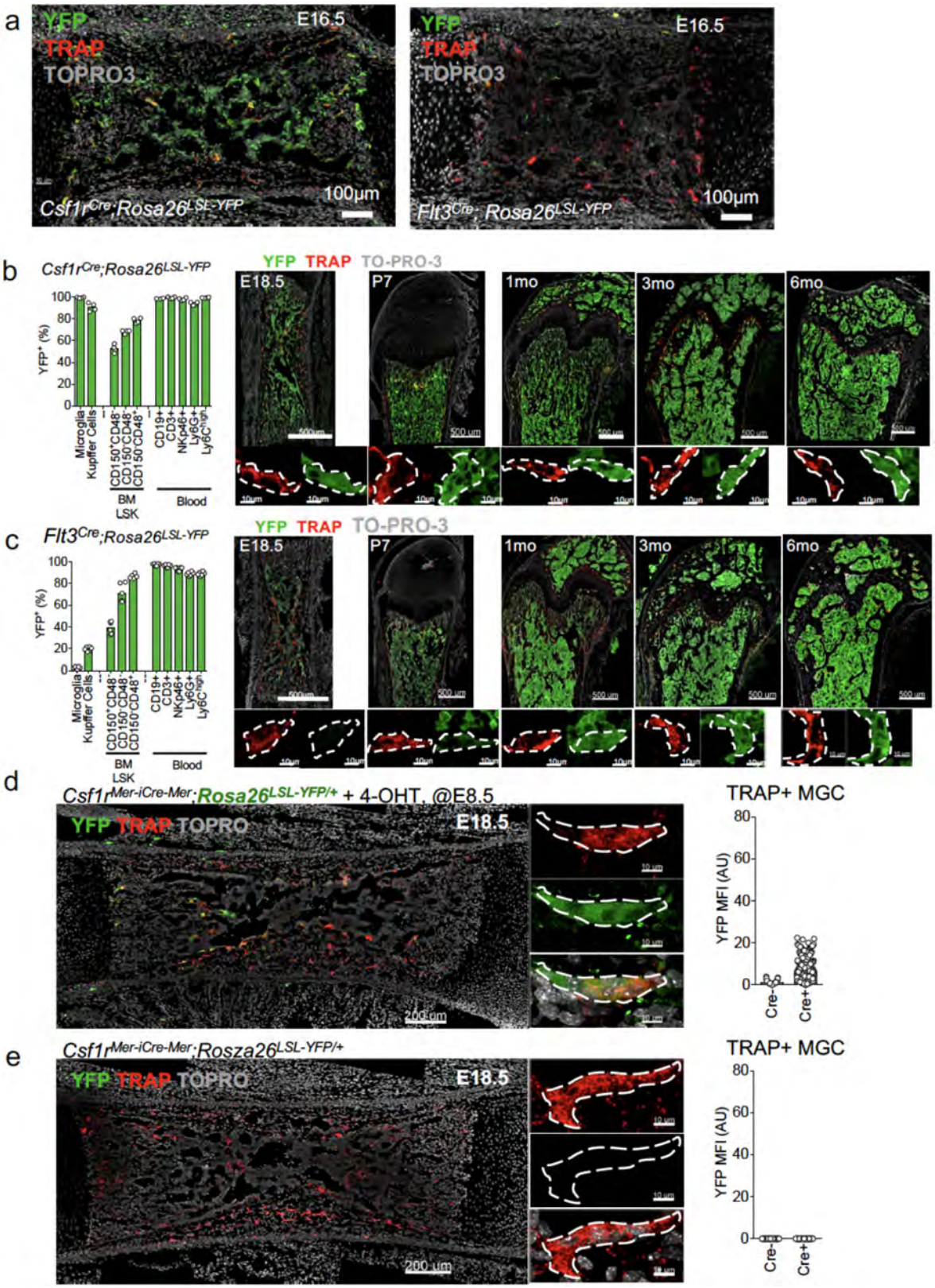

Extended Data Fig. 4 | See next page for caption.

Extended Data Fig. 4 | Colonization of the bone marrow by *Csf1r*$^{+}$ and *Flt3*$^{+}$ haematopoietic cells. a, Representative confocal microscopy of frozen sections from *Flt3*^{cre};*Rosa26*$^{LSL\text{-}YFP}$ and *Csf1r*^{cre};*Rosa26*$^{LSL\text{-}YFP}$ mice analysed at E16.5 ($n = 3$). **b**, YFP-labelling efficiency in *Csf1r*^{cre};*Rosa26*$^{LSL\text{-}YFP}$ mice analysed by flow cytometry in the indicated cell populations (left), and by confocal microscopy on frozen bone sections at the indicated age (right). Magnified regions (bottom right) show YFP expression in individual osteoclasts. YFP, YFP antibody; TRAP, ELF97 fluorescent substrate; TO-PRO-3, nuclear stain. **c**, YFP-labelling efficiency in *Flt3*^{cre};*Rosa26*$^{LSL\text{-}YFP}$ mice analysed as in **b**. Data in **b** and **c** are representative of at least three experiments per time point and genotype. Points represent individual mice. **d**, Genetic lineage tracing of osteoclasts in ossification centres using *Csf1r*$^{Mer\text{-}icre\text{-}Mer}$;*Rosa26*$^{LSL\text{-}YFP}$ mice. Representative high-power confocal microscopy of embryonic femurs showing MGCs in primary ossification centres from *Csf1r*$^{Mer\text{-}icre\text{-}Mer}$;*Rosa26*$^{LSL\text{-}YFP}$ E18.5 embryos pulsed with 4-OHT at E8.5, showing YFP expression in MGCs after Cre recombination (left) and quantified as MFI (right) from Cre^{+} ($n = 8$) and Cre^{-} ($n = 4$) (**d**), and unpulsed controls (**e**), showing the lack of YFP in Cre^{+} ($n = 4$) and Cre^{-} ($n = 4$). Sections were labelled with antibodies against YFP, TRAP (ELF97 substrate) and TO-PRO-3.

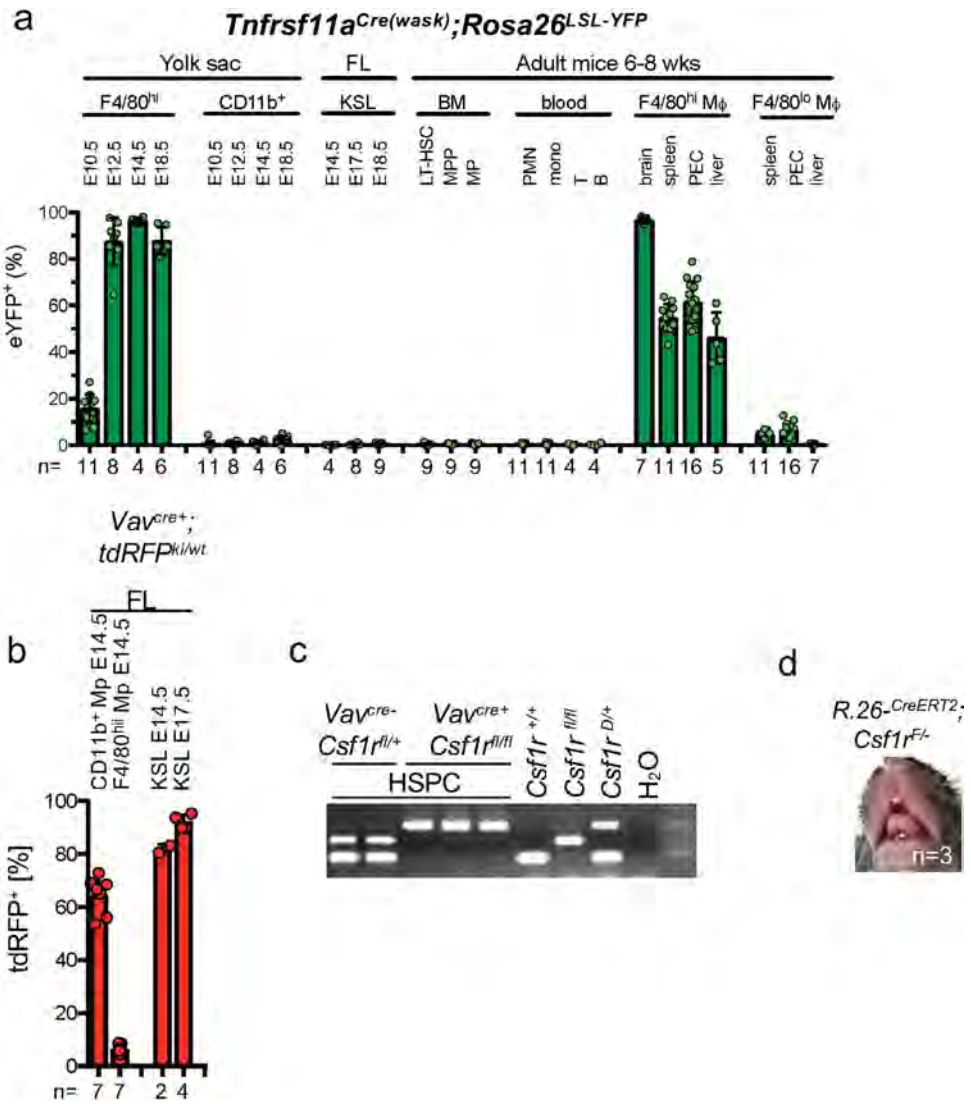

Extended Data Fig. 5 | *Tnfrs11a*$^{Wask\text{-}cre}$ knock-in mice enable deletion of target genes in fetal macrophages, but not in definitive HSCs and their progeny in blood and tissues, whereas *Vav*^{cre} mice enable deletion of target genes in definitive HSCs, but not in fetal macrophages. **a**, Bar graphs indicate percentage of cells expressing eYFP obtained by flow cytometry of *Tnfrsf11a*^{cre};*Rosa26*$^{LSL\text{-}YFP}$ cells from the indicated cell types, organs and time points. Data represent three independent experiments; *n*, number of mice per group indicated on *x* axis. **b**, Lineage tracing in the fetal liver of *Vav*$^{cre+}$;*tdRFP*$^{wt/ki}$ mice. *n*, number of mice per group indicated on *x* axis. **c**, Representative molecular analysis of *Csf1r* deletion in purified bone-marrow haematopoietic stem and progenitor cells (HSPC) from 62-week-old *Vav*^{cre};*Csf1r*$^{fl/fl}$ mice and controls ($n = 5$). **d**, Representative photograph of teeth from three-week-old *Rosa26-creER*$^{T2+}$;*Csf1r*$^{fl/-}$ pulsed with tamoxifen at E10.5 ($n = 3$ mice from 3 independent litters). FL, fetal liver; MP, myeloid progenitor; PMN, polymorphonuclear cells; mono, monocytes; T, T cells; B, B cells; PEC, peritoneal exudate cells. Data are mean ± s.d.; points represent individual mice.

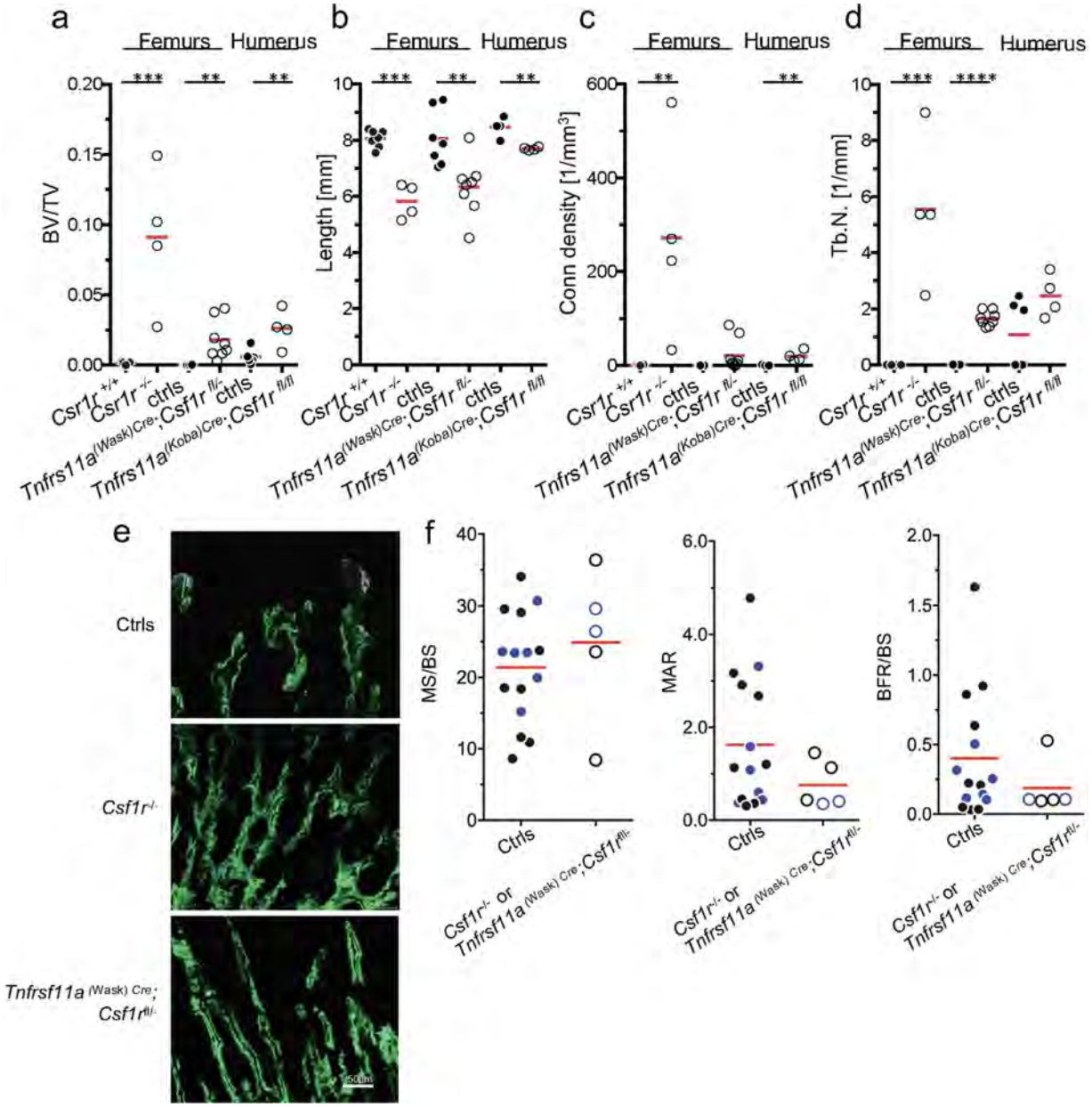

Extended Data Fig. 6 | Bone morphometric and dynamic histomorphometry effects of *Csf1r* deletion in *P21 Tnfrsf11a*^{cre}; *Csf1*$^{fl/fl}$ mice. a–d, Bone volume/total volume (BV/TV, **a**), bone length (**b**), connectivity density (**c**), and trabecular number (**d**) were analysed by micro-CT in 21-day-old mice. *Csf1r*$^{-/-}$ ($n = 4$), control littermates ($n = 7$); *Tnfrsf11a*$^{Wask\text{-}cre+}$;*Csf1r*$^{fll-}$($n = 8$), *Tnfrsf11a*$^{Wask\text{-}cre+}$;*Csf1r*$^{fll+}$ ($n = 7$), *Tnfrsf11a*$^{Wask\text{-}cre+}$;*Csf1r*$^{fll-}$($n = 3$) and control littermates ($n = 5$). **e**, Representative micrographs of calcein labelling (green) of femur of mice from the indicated genotypes and ages ($n = 4$). Scale bar, 50 μm. **f**, Quantification of calcein labelling by fluorescence microscopy: mineralized surface/bone surface, mineral apposition rate and bone formation rate/bone surface in *Tnfrsf11a*$^{Wask\text{-}cre+}$;*Csf1r*$^{fll-}$ *Csf1r*$^{-/-}$ ($n = 4$) and control littermates ($n = 15$). Data are mean ± s.d.; dots in graphs represent individual mice; *n* indicates the number of mice per group; unpaired two-tailed *t*-test. *$P \leq 0.05$, **$P \leq 0.005$, ***$P \leq 0.0005$ and ****$P \leq 0.0001$.

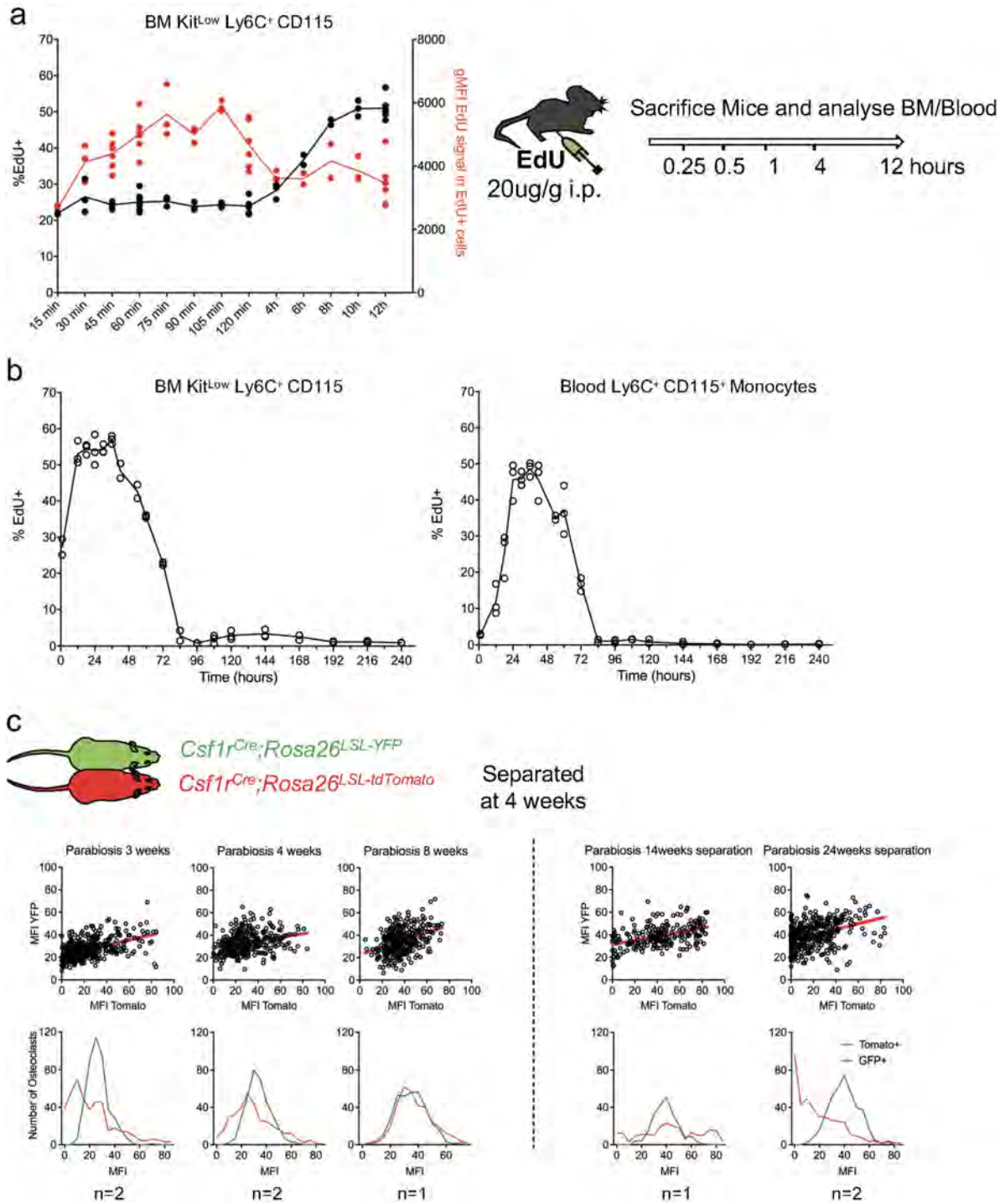

Extended Data Fig. 7 | EdU labelling of bone marrow myeloid cells. **a**, Short-term kinetics: EdU (20 μg g^{-1}) was injected intraperitoneally in C57Bl6/N mice at $t = 0$. Mice were euthanized at the indicated time points and the percentage of EdU^+ cells (blue) and the geometric MFI of EdU^+ cells (red) were determined by flow cytometry, showing rapid EdU incorporation. Percentage of EdU^+ cells plateaus at ~30 min, and geometric MFI plateaus at ~75 min. Following a first round of cell division, ~50% of monocytic cells are labelled after 8–12 h ($n = 3$–8 mice, see Source Data). **b**, Long-term kinetics: (1–240 h) EdU was injected as in **a** and percentage of EdU^+ monocytic cells in bone marrow (top) and blood (bottom) was determined by flow cytometry, showing labelling of ~50% of monocytic cells for ~2 days. Labelled cells were not detectable after three days. Points represent values from individual mice; data for each time point are pooled from two to three independent experiments (see Source Data). **c**, Parabiosis between *Csf1r*^{cre};*Rosa26*$^{LSL\text{-}YFP}$ and *Csf1r*^{cre};*Rosa26*$^{LSL\text{-}tdTomato}$ pairs as described in Fig. 3, paired for 1–8 weeks, and from *Csf1r*^{cre};*Rosa26*$^{LSL\text{-}YFP}$ partners separated after 4 weeks of parabiosis and analysed 4 weeks, 14 weeks and 24 weeks after separation. Scatter plots represent the MFI of individual $TRAP^+$ MGCs for YFP (*y* axis) and tdTomato (*x* axis), and histograms represent the overlaid distribution of the MFI values for YFP and tdTomato in $TRAP^+$ MGCs at the indicated time points. Data are mean ± s.d.; dots in graphs represent individual mice; *n* indicates the number of mice per group.

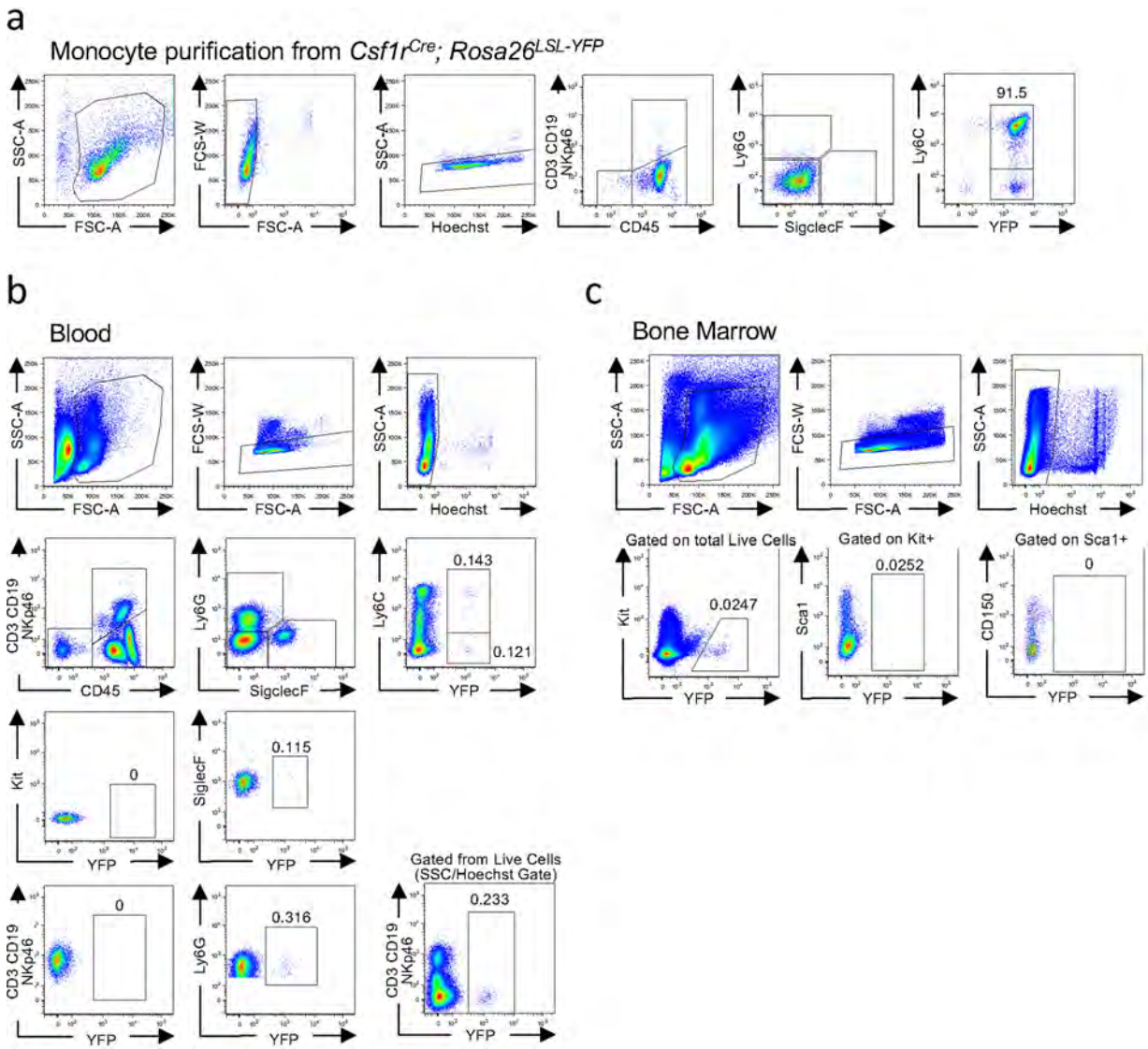

Extended Data Fig. 8 | FACS analysis of monocyte purification, and blood and bone marrow from transferred *Csf1r*^{cre};*Csf1r*$^{fl/fl}$ mice. **a**, Representative flow cytometry plots of purified bone marrow monocytes from magnetic-bead based enrichment; percentage of live YFP$^+$ monocytes is indicated. **b**, **c**, Representative flow cytometry plots from blood (**b**) and bone marrow (**c**) of 14-day-old mice transferred with 1×10^6 YFP$^+$ monocytes on day 5, 8 and 11; the percentage of YFP$^+$ cells is indicated. Results shown in **a**–**c** are representative of three independent experiments.

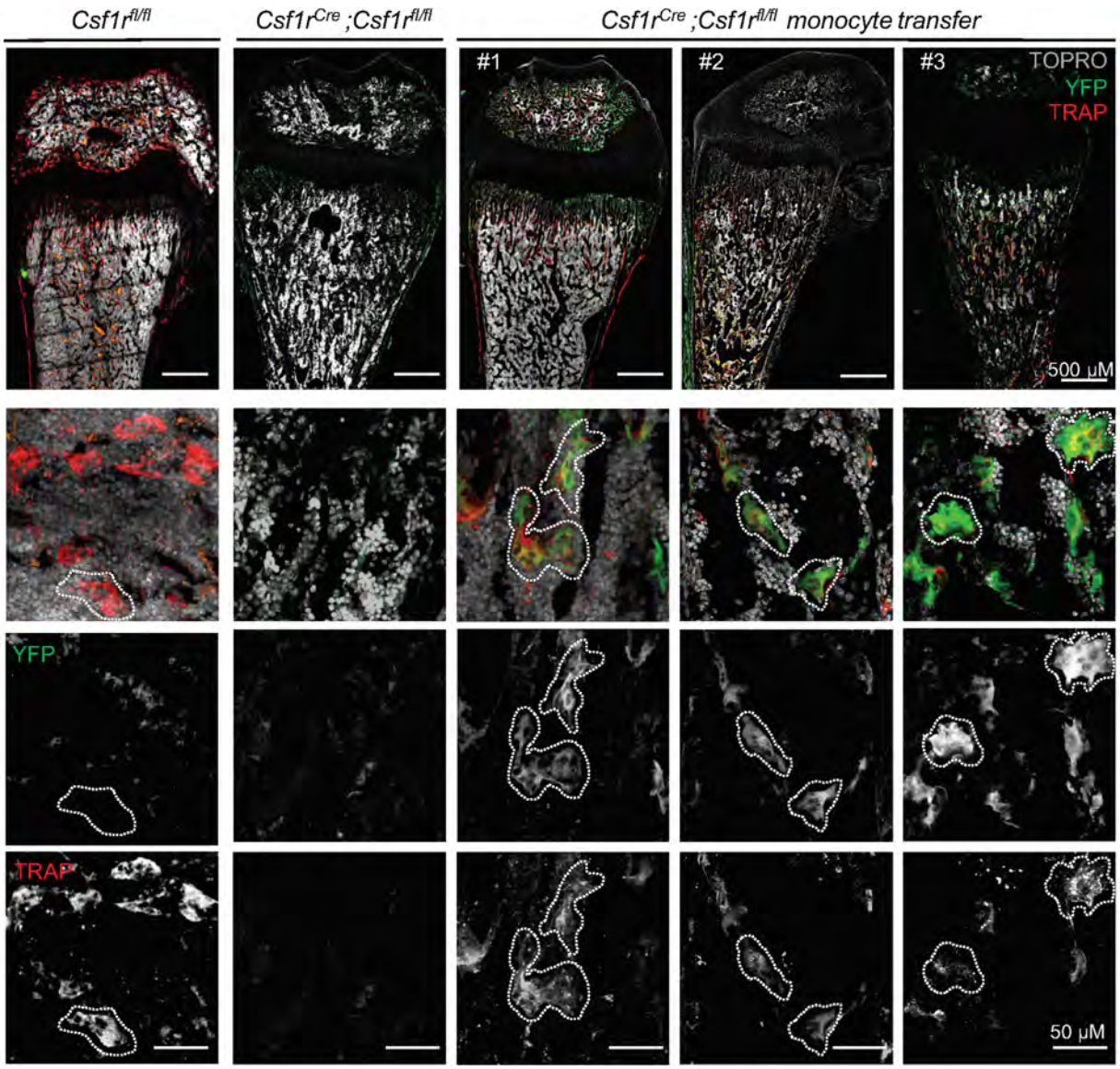

Extended Data Fig. 9 | Rescue of osteoclasts by monocyte transfer in *Csf1r*^{cre};*Csf1r*$^{fl/fl}$ mice. High-power confocal microscopy images of frozen sections from *Csf1r*^{cre};*Csf1r*$^{fl/fl}$ mice transferred with monocytes from *Csf1r*^{cre};*Rosa26*$^{LSL\text{-}YFP}$ and controls, stained with YFP antibody, TRAP substrate ELF97 and TO-PRO-3 nuclear stain. Examples of multinucleated TRAP^{+}YFP^{+} cells (osteoclasts) are indicated with dotted lines. $n = 3$ mice from independent litters. Numbers 1–3 correspond to the mice in Fig. 4d.

nature research

Corresponding author(s): Frederic Geissmann

Reporting Summary

Nature Research wishes to improve the reproducibility of the work that we publish. This form provides structure for consistency and transparency in reporting. For further information on Nature Research policies, see Authors & Referees and the Editorial Policy Checklist.

Statistical parameters

When statistical analyses are reported, confirm that the following items are present in the relevant location (e.g. figure legend, table legend, main text, or Methods section).

n/a	Confirmed	
☐	☒	The exact sample size (*n*) for each experimental group/condition, given as a discrete number and unit of measurement
☐	☒	An indication of whether measurements were taken from distinct samples or whether the same sample was measured repeatedly
☐	☒	The statistical test(s) used AND whether they are one- or two-sided *Only common tests should be described solely by name; describe more complex techniques in the Methods section.*
☐	☒	A description of all covariates tested
☐	☒	A description of any assumptions or corrections, such as tests of normality and adjustment for multiple comparisons
☐	☒	A full description of the statistics including central tendency (e.g. means) or other basic estimates (e.g. regression coefficient) AND variation (e.g. standard deviation) or associated estimates of uncertainty (e.g. confidence intervals)
☐	☒	For null hypothesis testing, the test statistic (e.g. *F*, *t*, *r*) with confidence intervals, effect sizes, degrees of freedom and *P* value noted *Give P values as exact values whenever suitable.*
☐	☒	For Bayesian analysis, information on the choice of priors and Markov chain Monte Carlo settings
☐	☒	For hierarchical and complex designs, identification of the appropriate level for tests and full reporting of outcomes
☐	☒	Estimates of effect sizes (e.g. Cohen's *d*, Pearson's *r*), indicating how they were calculated
☐	☒	Clearly defined error bars *State explicitly what error bars represent (e.g. SD, SE, CI)*

Our web collection on statistics for biologists may be useful.

Software and code

Policy information about availability of computer code

Data collection	NA
Data analysis	ZEN lite software (v2.6), Adobe Photoshop CS6, ImageJ (v1.52), GraphPad Prism (v7), In Vivo Scope 2.0, Imaris (Version 9.2)

For manuscripts utilizing custom algorithms or software that are central to the research but not yet described in published literature, software must be made available to editors/reviewers upon request. We strongly encourage code deposition in a community repository (e.g. GitHub). See the Nature Research guidelines for submitting code & software for further information.

Data

Policy information about availability of data

All manuscripts must include a data availability statement. This statement should provide the following information, where applicable:

- Accession codes, unique identifiers, or web links for publicly available datasets
- A list of figures that have associated raw data
- A description of any restrictions on data availability

Data are available from the corresponding author on reasonable request.

Field-specific reporting

Please select the best fit for your research. If you are not sure, read the appropriate sections before making your selection.

☒ Life sciences ☐ Behavioural & social sciences ☐ Ecological, evolutionary & environmental sciences

For a reference copy of the document with all sections, see nature.com/authors/policies/ReportingSummary-flat.pdf

Life sciences study design

All studies must disclose on these points even when the disclosure is negative.

Sample size	No statistical methods were used to predetermine sample size. For genetic fate-mapping and knockout models at least n=3 mice per group from 2 independent litters were analysed. We ensured that they were similar to those generally employed in the field.
Data exclusions	No data was excluded
Replication	All attempts for replication were successful and preformed by multiple investigators. Using independent litters of mice and Cre drivers.
Randomization	Male and female littermates were assigned into the control or knockout groups after genotyping
Blinding	The investigators were not blinded to allocation during following experiments and outcome assessment.

Reporting for specific materials, systems and methods

Materials & experimental systems

n/a	Involved in the study
☒	☐ Unique biological materials
☐	☒ Antibodies
☒	☐ Eukaryotic cell lines
☒	☐ Palaeontology
☐	☒ Animals and other organisms
☒	☐ Human research participants

Methods

n/a	Involved in the study
☒	☐ ChIP-seq
☐	☒ Flow cytometry
☒	☐ MRI-based neuroimaging

Antibodies

Antibodies used	All antibodies were published, and titrated prior to initial experiments. Listed in extended data table 2 and 3.
Validation	All antibodies used are common commercial clones that have been extensively used in the literature. We also titrated all antibodies prior to experiments.

Animals and other organisms

Policy information about studies involving animals; ARRIVE guidelines recommended for reporting animal research

Laboratory animals	Csf1riCre, Csf1rMeriCreMer, Csf1rflox, Csf1r-/-, Flt3Cre, Myb-/-, VavCre, Tnfrsf11aflox, Tnfrsf11a(Koba)Cre, Tnfrsf11a(wask)Cre, Ctsktm1(cre)Ska, R26-CreERT2, Rosa26LSL-YFP, Rosa26LSL-tdTomato. All ages are listed in the text when the animal was used, and additional information is located in the methods section under mice.
Wild animals	N/A
Field-collected samples	N/A

Flow Cytometry

Plots

Confirm that:

☒ The axis labels state the marker and fluorochrome used (e.g. CD4-FITC).

☒ The axis scales are clearly visible. Include numbers along axes only for bottom left plot of group (a 'group' is an analysis of identical markers).

☒ All plots are contour plots with outliers or pseudocolor plots.

☒ A numerical value for number of cells or percentage (with statistics) is provided.

Methodology

Sample preparation	For flow cytometry experiments, organs were incubated in PBS containing 1mg/ml collagenase D (Roche), 100U/ml DNase I (Sigma), 2.4mg/ml of dispase (Invitrogen) and 3% FCS (Invitrogen) at 37ºC for 30 min prior to mechanical disruption. Cell suspensions were centrifuged at 320g for 7 min, resuspended in FACS buffer (PBS, 0.5% BSA and 2 mm EDTA) containing purified anti-CD16/32 (1:100 dilution) and 5 % normal mouse, 5 % normal rat and 5 % normal rabbit serum and incubated for 15min at 4ºC. Samples were immunostained with antibodies mixes for 30 min at 4ºC.
Instrument	LSRFortessa
Software	Data was collected using DiVa 8.0.1 Software. Subsequent analysis was performed with FlowJo_v9.9.4. and v10.4
Cell population abundance	N/A
Gating strategy	FSC/SSC gates and dead cell stain (DAPI or Hoechst) were used to define single live cells. Doublets were removed based on FSC-A/FSC-W. In primary experiments all gates were defined based on FMO controls. In consecutive experiments, gates in fluorescence channels were drawn based on clear separation between negative and positive populations as shown in Supplementary Information

☒ Tick this box to confirm that a figure exemplifying the gating strategy is provided in the Supplementary Information.